Image Pan-sharpening with Markov Random Field and Simulated Annealing

Hailemariam Gedlu Kitaw

March, 2007

Image Pan-sharpening with Markov Random Field and Simulated Annealing

by

Hailemariam Gedlu Kitaw

Thesis submitted to the International Institute for Geo-information Science and Earth Observation in partial fulfilment of the requirements for the degree of Master of Science in Geo-information Science and Earth Observation, Specialisation: *Geoinformatics*.

Thesis Assessment Board

Thesis advisors	Dr. V. A. Tolpekin Prof. Dr. Ir. A. Stein
Assessment Board Chair	Prof. Dr. J.L. van Genderen
External examiner	Dr. Ir. L.J. Spreeuwers

INTERNATIONAL INSTITUTE FOR GEO-INFORMATION SCIENCE AND EARTH OBSERVATION

ENSCHEDE, THE NETHERLANDS

Disclaimer

This document describes work undertaken as part of a programme of study at the International Institute for Geo-information Science and Earth Observation (ITC). All views and opinions expressed therein remain the sole responsibility of the author, and do not necessarily represent those of the institute.

Abstract

As many earth observation satellites provide both high resolution panchromatic and low resolution multispectral images, pan-sharpening is an important technique in the field of remote sensing to produce a high resolution multispectral image for a given low resolution multispectral image and a higher resolution panchromatic image of the same area. To date, several image pan-sharpening techniques like the IHS method, the PCA method, the wavelet method, etc have been developed. However for the recent high and very high resolution satellite images the developed algorithms can hardly produce satisfactory results [44, 45]. There are significant color distortions in the pan-sharpened image and the quality of these pan-sharpened images is also seldom questioned.

This research concentrates on developing a new method for image pan-sharpening in *Bayesian* image restoration framework using *Markov Random Field (MRF)* and *simulated annealing* that provide *maximum a posteriori (MAP)* estimate of the pan-sharpened image. The study models the (unknown) pan-sharpened image with an MRF (prior probability) and models observation process for the panchromatic and the coarse resolution multispectral images (conditional probability). These probabilities are combined to derive posterior probability for the pan-sharpened image. Optimal solution is sought as the image that maximizes the posterior probability. The simulated annealing algorithm is used to obtain the optimal solution.

In order to test the performance of the method, a reference image is chosen and is assumed as the unknown pan-sharpened image. The reference image is degraded to produce panchromatic and multispectral images. The method is then applied to restore the pan-sharpened image from these degraded images and the accuracy assessment is performed by comparing it with the reference image. The method shows a very high correlation between the restored pan-sharpened image and the reference image. The performance of the proposed method is compared with other pan-sharpening methods and is proved that it performs better than existing methods.

Keywords

super resolution, QuickBird, Bayesian image restoration, IKONOS, high resolution, image fusion, Pan-sharpening, Simulated Annealing, Markov Random Field (MRF)

Contents

List of Tables

List of Figures

Acknowledgements

This research wouldn't have reached to a successful completion without the help, support and encouragement of many individuals, who deserve my acknowledgement. First, I thank my first supervisor *Dr. V. A. Tolpekin* for his tireless effort and constructive comments that give brightness to this work. I would like to express my sincere gratitude for his careful guidance, suggestions and contributions throughout the thesis period. I want to extend my appreciation to my second supervisor *Prof. Dr. Ir. A. Stein* for his critical comments and advice that enhance this work.

I would like to thank the Netherlands government for granting me the NFP scholarship for this study. I express my sincere gratitude to my employer Arba Minch University for facilitating and giving me permission to undertake this study.

I am very grateful to my GFM 2, 2005 colleagues for their friendship over the last 18 months study period. I am thankful to my Ethiopian colleagues for the company and moral support during the hard times.

My heartfelt gratitude goes to my lovely mother *Abebech Kibret*, to my sisters, and especially to my brother *Endalamaw Gedlu* for all their special love, care, thoughtfulness and encouragement. Without them I wouldn't have gone this far. Last but not least, I am very grateful to my love *Essete Aberra* for her love, kindheartedness, encouragement and being with me in spirit all this 18 months.

Above all, I would like to give all the praise to the *Almighty God*, who made me *His* creature and gave me *His* divine grace to successfully accomplish this study; all this wouldn't have been possible without *His* will. *Lord*, Thank you !!

Hailemariam Gedlu
March, 2007.

"To *God* be the glory, for the great things he has done"

Chapter 1

Introduction

1.1 Background

Image data from Earth observation satellites contain huge amount of information about the Earth surface. Some of these satellites, such as QuickBird, IKONOS, Landsat 7, IRS, SPOT, offer both panchromatic images at a high spatial resolution and multispectral images at a lower spatial resolution. Combination of such different data sources provides more information than the source images separately. In order to make use of the benefits from such a combination, numerous image fusion techniques have been developed and used in many applications.

Wald , L. [39] defined image fusion as "a formal framework which are expressed means and tools for the alliance of data of the same scene originating from different sources. It aims at obtaining information of greater quality; the exact definition of quality will depend upon the application." It improves the quality of information better than what can be obtained from only one type of data. Fused images give a better interpretation means and results as data with different characteristics are merged. The main aim of image fusion is to integrate different and matching data to enhance the information in the images and also to increase the reliability of interpretation. It is very important in many applications of remote sensing. It can be used to sharpen images, improve geometric corrections, provide stereo-viewing capabilities for stereophotogrametry, enhance certain features, complement data sets for improved classification, detect changes using multitemporal data, substitute missing information, replace defective data etc.[31]. In addition to the field of earth science it is used in medical sciences especially for diagnosis. It is used for modeling the human body or treatment planning [12, 39] .

Due to the fact that it is impossible to obtain a higher resolution multispectral image from a sensor, most image fusion methods focus on the use of information from both panchromatic and multispectral images. In this research high or low "resolution" refers to the spatial resolution of images unless it is mentioned. Multispectral image data contain significantly more spectral information than a panchromatic data, and a panchromatic image data of the same area has a

higher spatial resolution than the multispectral data.

Image fusion can be performed at three different levels: at pixel level, at feature level and at decision level [12, 37]. Fusion at pixel level is the lowest level and uses raster data that is at least co-registered. The role of geocoding is very important as it avoids mis-registration that causes artificial colors.

Image pan-sharpening is a pixel level fusion technique that describes a process of changing a set of low (coarse) spatial resolution multispectral images to high (fine) spatial resolution color images, by fusing a co-georegistered fine spatial resolution black/white (panchromatic) image of the same area. The panchromatic image is usually obtained from the same platform and taken at the same time or in a very short time duration with the multispectral image [42]. It is a fusion technique that takes place at pixel level of the high resolution mainly to increase the spatial resolution of the multispectral image via the higher resolution pan image. At the same time it aims at preserving the spectral information in the multispectral data [12]. It is also refereed as resolution merge, image integration, image fusion, and multispectral data fusion [37]. The term pan-sharpening is preferred and used in this research as it is more clearly and specifically defined.

Pan-sharpening has become very important in many applications of remote sensing like for land use classification, for detecting changes, for updating maps, for monitoring hazards and for many other applications. Pan-sharpened images can also be used for visualization purposes. But for quantitative spectral measurements different quality level is required. An other interesting application of pan-sharpening is in the enhancement of multispectral images for color televisions. Conventional color imaging science is based on the paradigm that three variables are sufficient to characterize a color. Color television uses three color (multispectral) channels. Mainly the multispectral signals have a defined spectral band and a lower resolution than panchromatic signals. This is because multispectral signals contain fewer photons and they need larger detectors for similar exposure periods. Due to this fact three color channels are often insufficient for high quality imaging like for museum applications. Recently researches on pan-sharpening has been done to introduce imaging technologies with more than three channels [19, 30]. The methods utilize the panchromatic signal to increase the resolution of the multi-spectral signals to provide an increased resolution color output.

Image pan sharpening can be considered in the context of image restoration framework [24]. High spatial resolution multispectral image is assumed to exist, but it is unknown and observed through “degraded” images. The degraded observed images are a panchromatic image degraded spectrally and a multispectral image degraded spatially. The task is then to restore the assumed “true” image. This is a type of an ill-posed problem (in Hadamar sense) where there exists no unique solution and/or small variations in the observed images may result in large variations in the resulting image. Therefore it has to be

regularized, which can be done by incorporating the prior information using the Markov Random Field (MRF) approach.

The Markov Random Field (MRF) is a useful tool for analyzing and integrating contextual information and considers this contextual information as a prior information in image analysis. It is a probabilistic model defined by local conditional probabilities. Contextual models are one way to model prior information and MRF theory can be applied to model a prior probability of contextual dependent patterns, such as textures and object features [24]. Spatial context is simply meant for the correlations between spatially adjacent pixels in a spatially neighboring pixels [35]. Spatial context of a multispectral image provides a way to improve the separation between ground cover classes as compared to a single image analysis. In an image a pixel classified as a "water body" is most likely surrounded by pixels of the same class and is unlikely to be surrounded by neighbors from other classes. That means using the concept of context, pixels can not be treated in isolation, rather they are considered to have a relationship and being statistically dependent with their neighbors. So then by fusing a data with a priori image model (which is in fact used to describe the expected association or relation ships between the neighboring pixels), spatial information can be included [12].

In statistical modeling Bayesian theory is a way to incorporate prior information. Its key elements are the prior and the conditional probability density function. By combining these functions a value can be expressed in terms of a *maximum a posteriori (MAP)* criteria. *MAP* probability is one of the most popular criteria for optimality [36]. There are many MAP-MRF optimization algorithms. Two iterative algorithms, namely simulated annealing (SA) and maximizer of posterior marginals (MPM) are well known in literature [24, 26].

Various factors should be considered before image pan-sharpening is done. The application of the pan-sharpened image to be used, co-registration, the viewing angle of imagery, the resampling methods are the major ones to be thought first. Since many satellite images are available and can be used for image pan-sharpening, knowledge of the main application of the pan-sharpened image helps in selecting the kind of data to be used. Co-registration is one of the most important preprocessing steps that should be done before pan-sharpening to avoid artifacts of the final pan-sharpened image. In order to get a desired result the viewing angle of imagery should also be carefully set especially if the multispectral and the panchromatic images are taken at different times. A suitable resampling technique should also be used during geometric projection, geometric correction and co-registration. The need for the technique of pan-sharpening arises mainly because of the fact that the designing of a sensor to give both high spatial and spectral resolution is restricted by the tradeoff between spectral resolution, spatial resolution and signal-to-noise ratio of the sensor [37]. The multispectral image with high spatial resolution is preferable in many applications.

1.1.1 Image resolution

Remote sensing image data are beyond a picture, they are measurements of electromagnetic energy. The characteristics of sensor platform system determine the quality of image data. The four characteristics that determine the quality of an image data are the spectral characteristics, the spatial characteristics, the radiometric characteristics and the temporal characteristics. These four characteristics can also be further specified by their coverage and their resolution (defined as the smallest units that can be distinguished) [8].

Based on the resolution characteristics space born systems can be grouped into low resolution systems (with spatial resolution of 1 km to 5 km) like Meteosat-8 and NOAA-17, medium resolution systems (with spatial resolution of 10 m to 100 m) like Landsat-7 and Terra, and high resolution systems (with a spatial resolution better than 10 m) like SPOT-5, Resourcesat-1, IKONOS and QuickBird [8, 42]. IKONOS and QuickBird are the latest high resolution satellites that collect simultaneously multispactral images (MS) at a lower spatial resolution (4m and 2.8m respectively) and panchromatic (Pan) images at a higher spatial resolution (1m and 0.7m resolution). In these satellites most urban objects can be recognized because of the color differences in the multispectral images, but one can not exactly demarcate and do further analysis because of lack of spatial resolution. However the shapes of objects can be clearly identified from the panchromatic images but due to lack of spectral information further image analysis can not be done precisely.

Spectral resolution

The width within the electromagnetic spectrum that can be sensed by a band in a sensor is called the spectral resolution. It is the width of the spectral wavelength bands that the sensor is sensitive to [8, 37]. The spectral resolution becomes better as the spectral band width becomes narrower. With a higher spectral resolution image it is possible to define finer wave length intervals and hence it is possible to compare and identify specific classes, features or objects easily. If the sensor has a few spectral bands, they are called multispectral; and hyperspectral if the number of spectral bands is in hundreds.

Both color and Black & white films record wavelengths including over much or all of the visible part of the electromagnetic spectrum. Since most of the wavelengths of the visible spectrum are not individually separated and overall reflectance in the entire visible portion is recorded in black and white film, its spectral resolution is low. Whereas since color film is individually sensitive to the reflected energy at the blue, green, and red wavelengths of the spectrum it has a higher spectral resolution. That means it can represent features of different colors based on their reflectance [1]. Table 1.1 shows the spectral information for IKONOS and QuickBird satellites.

Table 1.1: *Spectral band information of IKONOS and QuickBird Satellites*

IKONOS		*QuickBird*	
Band Name	*Spectral Band) (nm)*	*Band Name*	*Spectral Band (nm)*
Pan	525.8 - 928.5	Pan	450 - 900
MS-1 (Blue)	444.7 -516.0	MS-1 (Blue)	450 - 520
MS-2 (Green)	506.4- 595.0	MS-2 (Green)	520 - 600
MS-3 (Red)	631.9 - 697.7	MS-3 (Red)	630 - 690
MS-4 (VNIR)	757.3- 852.7	MS-4 (VNIR)	760 - 900

Spatial resolution

The spatial resolution of an imaging system is not an easy concept to define. It can be measured in a number of different ways depending on the user's purpose. The criteria that use to define this concept are the geometrical properties of the imaging system, the ability to distinguish between point targets, the ability to measure the periodicity of repetitive targets, and the ability to measure the spectral properties of small targets [27]. The most commonly used measure based on the geometrical properties of the imaging system is its instantaneous field of view (IFOV). The IFOV determines the ground area which is recorded by a sensor at a given instant of time. A cross-section of the recorded or imaged intensity distribution of a single point source corresponds to a Gaussian-type distribution. This distribution function is called the point spread function (PSF). The point spread function describes the response of an imaging system to a point source or point object. The PSF is also determined by atmospheric effects. In this definition spatial resolution refers to the smallest unit-area measured. It indicates the minimum detail of objects of an image that one can detect. So as the spectral resolution is dependent on the width of the spectral band, the spatial resolution is dependent on the IFOV. As the IFOV becomes finer, the higher is the spatial resolution [8, 12, 37]. Spatial resolution of an image is also understood as the clarity of the high frequency detail information that is available in an image [37]. The detail of an image becomes better and clearer if the spatial resolution is higher.

Relationship between signal to noise ratio, and spectral resolution & spatial resolution

Signal to noise ratio abbreviated as SNR is defined as the ratio of a given transmitted signal (that is the meaningful information) to the background noise involved in the measurement process. This ratio is common in most imaging sensors based on their design and the sensors recognize the energy that is reflected only if the background noise ratio is greater than the designed value [37]. So the minimum signal sensitivity of the sensors is determined by the SNR value.

It is mentioned in the above sections that narrow bandwidths are common in multispectral and hyperspectral images. That means in order to gather enough signal to overcome the minimum signal sensitivity of the sensor, such images need a coarser IFOV or a low spatial resolution. A similar argument also holds true for panchromatic images. That is to gather enough signal strength the spectral band width should be larger. That is why only spectral resolution and spatial resolution are usually discussed in literature. The other one (i.e. the SNR) is fixed based on the design constraint [15, 37]. Such a constraint can be controlled using image pan-sharpening techniques that can produce images with both high spatial and high spectral resolution.

1.2 Problem statement

Due to high interest for pan-sharpened images, numerous pan-sharpening algorithms have been developed by researchers, and some of them have been integrated in commercial remote sensing software packages like ERDAS Imagine and ENVI. Many researchers find fusion and sharpening in particular just non-scientific and not well-grounded procedures, e.g. [44]. Recently Vijayaraj [37] has done a quantitative analysis of pan- sharpened images of the most well known methods on different types of data. The most well known image pan-sharpening methods, especially that are efficient for Landsat TM and SPOT images, are the intensity-hue-saturation (IHS) transformation method, the principal component analysis method, the Brovey transform method and the latest wavelet transform method [12]. The latest wavelet transform method for image pan-sharpening has been discussed on different literature sources mainly because of its being more advantageous than the other methods [20, 37, 43]. At the moment most of the available pan-sharpening methods are not efficient when dealing with the new commercial high resolution satellite images like IKONOS and QuickBird [44, 45]. The quality of the pan-sharpened image of these satellite images is seldom questioned by those people who use it. Some researchers have mentioned that the results of the pan-sharpened images using the different methods have a significant color distortions and there are only a few pleasing outcomes [7, 22, 37] on these types of images. Therefore this study focuses on developing a new Bayesian method for image pan-sharpening using the Markov Random Field and the simulated annealing algorithm and assesses its quality for satellite images.

1.3 Research objectives

The general objective of this research is to come up with a new Bayesian method for satellite image pan-sharpening using the Markov Random Field Approach (MRF) and the simulated annealing that can give a *maximum a posteriori (MAP)* estimate of the pan-sharpened image. The sub-objectives are:

1. To formulate pan-sharpening as an image restoration model and to determine the parameters of this model by building observation and prior

models.

2. To integrate the modeled prior information with the conditional information obtained from the multispectral and the panchromatic images using the Bayesian estimation in order to get the final pan-sharpened image and to find the optimal solution using the simulated annealing algorithm.

3. To assess the quality of the pan-sharpened image and,

4. To compare the new method with the already existing methods of pan-sharpening.

The result of this research will provide image analysts, most notably from the geo-informatics society with an efficient method for image pan-sharpening and obtain more information from remotely sensed data. It will also be useful in many applications of remote sensing especially to users of high resolution satellite images to obtain better qualities of information that would come as a result of the increase in spatial resolution; and gives awareness of the quality of pan-sharpened products and consequences of using them in quantitative analysis.

1.4 Research questions

In line with the above mentioned research objectives the following research questions are formulated in order to meet the objectives:

1. How to model the prior and the conditional information that are used to obtain the *maximum a posteriori (MAP)* result?

2. What are the parameters that are necessary to use in modeling the prior information and the conditional information and how to estimate these parameter values from the data?

3. How to define the quality of the final result?

4. How to compare the quality of the pan-sharpened image with other methods of pan-sharpening?

1.5 Research setup

The adopted setup is carried out in five phases: pre-processing, modeling of the prior information, modeling of the two conditional information, estimation of the *maximum a posteriori (MAP)*, quality assessment and performance comparison. The flow chart for all of the phases is shown in figure 1.1.

1.5.1 Phase 1 - Pre-processing

In this phase some pre-processing steps including co-registration and resampling to common grid are performed (usually done by the data provider).

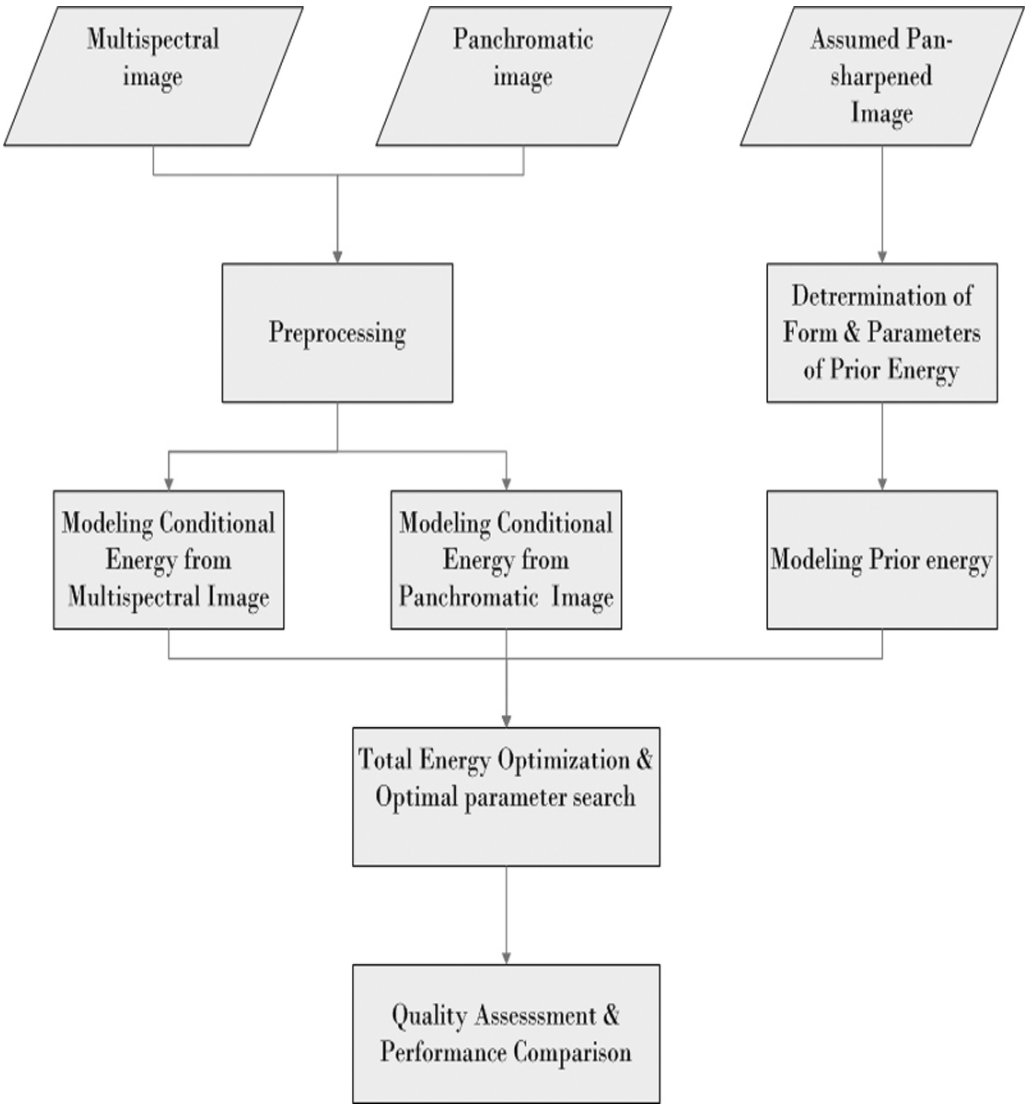

Figure 1.1: *Flow chart of the research.*

1.5.2 Phase 2 - Modeling the prior information

The prior information (energy) is modeled from the assumed high resolution multispectral image using the Markov Random Field (MRF). The suitable parameters and form of the model are set to generate the contextual information.

1.5.3 Phase 3 - Modeling the conditional information

The second stage of the method is to model the two conditional probabilities that can be obtained from the two spatially and spectrally degraded images. A model developed by Alvarez *et al.*[9] is used to model the two conditional information.

1.5.4 Phase 4 - Estimation of the MAP

In this phase the two conditional energies and the prior energy obtained from the previous phases are integrated under the Bayesian framework in order to get the maximum probability that will be used to get optimal solution for the pan-sharpened image. Some of the optimization methods include, iterated conditional modes, stochastic relaxation (which is a form of Simulated Annealing), the highest confidence first (HCF) etc [13]. The Simulated Annealing method of approximation is adopted to get the *maximum a posteriori (MAP)* estimate for the pan-sharpened image that maximizes the posterior probability. Proper parameters will be sought to get optimal solution for the pan-sharpened image.

1.5.5 Phase 5 - Quality Assessment and performance comparison

For assessing the quality of the pan-sharpened image a multispectral IKONOS image is assumed as a true pan-sharpened image. Two artificial images are prepared from this existing IKONOS image. It is degraded it into multispectral and panchromatic images and a pan-sharpened image is restored from these two degraded images. The quality of this pan-sharpened image is assessed by comparing the reference image with the restored image on a pixel-by-pixel level using statistical measures like correlation coefficients and the root mean square error. A comparison between the method and other methods of pan-sharpening is done using the statistical measures. In a separate experiment, a QuickBird image with an aerial photograph is compared visually.

1.6 Structure of the thesis

This research thesis contains six chapters. The ***first chapter*** describes the background, the problem statement, the objectives, the research questions and the approach of the research. ***Chapter two*** presents a literature review on the previous works of MRF in the field of remote sensing and a brief review of existing image pan-sharpening techniques. ***Chapter three*** describes the data types and data sets used for this study and the preprocessing steps employed. ***Chapter four*** discusses the new MRF-SA method developed in this study. ***Chapter five*** presents the results of the research for both the synthetic and remote sensing images followed by analysis and discussion. Finally ***chapter six*** depicts conclusion of this study and gives recommendation for further research.

Chapter 2

Literature review

This chapter briefly explains previous works of MRF in the field of remote sensing and reviews existing pan-sharpening techniques.

2.1 Previous works of MRF in remote sensing

In the field of remote sensing the main application of the Markov Random Fields is to model contextual relationships in image analysis. The first work of MRF for image analysis was on MRF based statistical methodology for image analysis done by Geman and Geman [18]. Since then MRFs are used in many applications like image segmentation [18], filtering (denoising) [25], classification of remotely sensed data [36], change detection [11, 21] and super resolution land cover mapping [21].

Solberg and et al. [35] developed an MRF-based algorithm for multi-source classification of remote sensing data. They studied that additional source in addition to the information that can be obtained from individual sensors can provide complementary data. They considered pixels in context with other measurements to get more complete information. They merged the spatial and temporal contextual information within the framework of their model. Based on the experimental results they made they proposed MRF model for classification of multi-source satellite imagery.

Bruzzone et al. and Kasetkasem et al. developed methods for detecting changes in the year 2000 and 2002 respectively [11, 21]. The first authors modeled two automatic change detecting techniques. Mainly their approach is based on MRF models that consider inter-pixel dependence. Kasetkasem et al. also employed an MRF model to detect changes. Their basic idea is that changes are more likely to occur in connected regions rather than at disjoint points. They used the MRFs in their method to use additional information from observed image data and estimated the *maximum a posteriori (MAP)* solution to search for the global optimum.

Super resolution mapping (SRM) is an other work that used the MRFs. It works

by dividing the coarse pixel into subpixels and to each corresponding subpixels it gives an estimate for the class proportion using subpixel classification. Then class labeling is optimized using the principle of spatial dependency [33]. There are few super resolution methods and among them Markov random field (MRF)-based SRM is one of the most recently introduced techniques. Its suitability is also assessed in a systematic way very recently.

The importance of MRF to integrate contextual information at pixel level is shown in all the above applications of MRF in the field of remote sensing. The next section briefly presents some existing techniques of image pan-sharpening.

2.2 Image pan-sharpening techniques

A number of pan-sharpening techniques have been developed by many authors and can be found in many literatures. Recent works include the interband structure modeling for pan-sharpening of very high resolution [15], remote sensing image fusion using the curvelet transform [26], An MTF-based spectral distortion minimizing model for pan-sharpening of very high resolution multispectral images of urban areas and few others [10]. In the last few years a comprehensive revision and analysis [10] of the most well known and published image pan-sharpening methods have been developed. Most of these known methods are successful especially on Landsat TM and SPOT images. Yun Zhang [10] generally categorized these methods in to three groups: the projection and substitution methods (like the Intensity-Hue-Saturation and the Principal component analysis methods), the band ratio and arithmetic combinations (like the Brovey method), and the different wavelet fusion methods which are the recent "best" methods. In addition to these three groups, other pan-sharpening methods using the Bayesian paradigm have also been developed recently using different models.

2.2.1 The Intensity-Hue-Saturation (IHS) method

The Intensity-Hue-Saturation method for image pan-sharpening is based on the Intensity-Hue-Saturation transform. The transformation separates the intensity information from the color carrying information [34]. A pure color is described by a hue and the degree to which this pure color is diluted by a white light is called the saturation [8]. The Intensity-Hue-Saturation transform helps to separate the spatial information into a single intensity band. Among the different transformations that differ in computing the intensity component, Smith's hexacone and triangular models are the most widely known and used ones [37]. The maximum value of red, green and blue ($I = max(R, G, B)$) is taken as the intensity value in the hexacone model and one third of the sum of the red, green and blue values ($I = 1/3(R + G + B)$) is taken as the intensity value in the case of the triangular model. Since the hexacone model ignores two of the values, the computed intensity value may not be representative of the information. The best suited and preferred transformation model for image

fusion is the triangular model.

There are different models of the Intensity-Hue-Saturation (HIS) method for image pan-sharpening. The basic idea is as follows. First the multispectral image composite is changed from the RGB color space to the HIS color space domain. Then the intensity element which is the spatial component is substituted by using the histogram matched (higher resolution) panchromatic image. At the same time the hue and the saturation parts are resampled to the resolution of the panchromatic image. Lastly the inverse IHS transformation is used to get back into the RGB color domain to obtain a fused image [10, 15, 38, 41]. Satisfactory result can be obtained therefore if the intensity of the image of the HIS transform has a high correlation to the panchromatic image used to be fused. Due to the fact that the musltispectral and panchromatic images obtained from IKONOS and QuickBird have very low correlation there is a color distortion in the final outcome particularly when the bands 1, 2 and 3 are fused with the panchromatic image [10].

2.2.2 The principal component analysis (PCA) method

The principal component analysis method for pan-sharpening abbreviated as PCA is the other known method of image pan-sharpening that belongs to the projection and substitution method categories. Principal component analysis can easily be understood as the transformation of correlated variables into a set of uncorrelated variables called principal components. It is possible to have as many possible principal components as there are variables [37]. The computation of the principal components involves the usage of the eigenvalues and eigenvectors of the covariance matrix of the bands of the multispectral image. The variance along the principal components is represented by the eigenvalues and the direction of the principal components is represented by the eigenvectors. Then by arranging the eigenvectors in the order that corresponds to the eigenvalues the transformation matrix for finding the principal components will be obtained. So the direction of the highest eigenvalue or maximum variance belongs to the first principal component and the second maximum variance will be represented by the second principal component and so forth [17, 34, 37].

So what the PCA method of image pan-sharpening does is that after the PCA is applied to the multispectral image bands to compute the principal components, the first principal component is substituted with the resolution panchromatic image. Later in order to go back to the domain of the image the inverse PCA transform is done [7, 12, 15]. The PCA sharpening method is sensitive to the area to be sharpened. The performance of the method varies with images having different correlation between the multispectral bands. The major problems of this technique on the high resolution satellite images are dominant spatial information and weak color information. This is mainly because the variance of pixel values as well as the correlation between bands are different depending on the land cover; but the first principal component that is replaced by the pan image has a high variance and this favors the pan image to increase its effect

on the final outcome [10, 12].

2.2.3 The Brovey transform method

The Brovey transform is the other known method of pan-sharpening that is under those categories of techniques that use the band ratio and arithmetic combinations. It is named after its author and uses ratios to sharpen the multispectral (MS) image [12]. The basic idea in short is as follows. It first calculates the ratio between a panchromatic cell value and the average of the corresponding multispectral cell values and uses that ratio to compute the color component values for the pan-sharpened result [1, 7]. It is expressed as:

$$DN_{fusedMS_i} = (\frac{DN_{bi_i}}{DN_{b_1} + DN_{b_2} + ... + DN_{b_n}})DN_{PAN} \tag{2.1}$$

where DN is the digital number of a particular band and b_i represents a particular band of the multispectral image. On the high resolution satellite images this method has in fact a nice contrast but the spectral characteristic is greatly artificial and hence there is a color distortion on the final output [7, 12].

2.2.4 The wavelet methods

The wavelet image fusion methods are among the latest techniques for image pan-sharpening. It is based on the mathematical tool widely used in image analysis called the wavelet transform. There are few wavelet-based pan-sharpening methods available in most well known literature sources [7, 12]. All of them are developed based on the powerful mathematical tool mostly used in signal analysis called the wavelet transform that decomposes an image into various images with different spatial resolutions [29, 37]. By using the discrete wavelet transform (DWT), a function $f(t)$ in one dimension can be represented by:

$$f(t) = \sum_{j,k} a_{j,k}\psi_{j,k}(t) \tag{2.2}$$

where $a_{j,k}$ are the wavelet coefficients,

$\psi_{j,k}(t)$ are the basis functions of scale j and translation k of the function called the mother wavelet $\psi(t)$.

For a two dimensional DWT, the function is just an extension of the one dimensional DWT that is obtained by applying the DWT across rows and columns of an image independently. It is represented as:

$$f(x,y) = \sum_{k,l} C_{J_0}[k,l]\,\phi_{j,k,l}(x,y) + \sum_{S=H,V,D}\sum_{j=J_0}^{\infty}\sum_{k,l} D_j^S[k,l]\,\psi_{j,k,l}^S(x,y) \qquad (2.3)$$

where C_{J_0} is the approximation coefficients,
$\phi_{j,k,l}(x,y)$ is the scaling function,
D_j^S is the set of detail coefficients,
$\psi_{j,k,l}^S$ is the set of wavelet function and
j,k,l represents the horizontal, vertical and diagonal subspaces

The basic idea of the wavelet-based pan-sharpening methods is as follows. The first step is to decompose the low resolution multispectral image into high resolution panchromatic images using the wavelet transform coefficients. As the wavelet coefficients go from finer scale to coarser one, they are of lower spatial resolution. The second step is to look for a low resolution pan image and replace it with one of the multispectral band that has the same level of resolution. The last step is just to carry out an inverse wavelet transform in order to convert the result of the second step to the original panchromatic resolution level [7, 12]. This method is relatively the most successful one especially on Landsat TM and SPOT images and the color distortion on the high resolution satellite images is smaller than the other methods. In many literature sources it is also noted that it is computationally intensive and there is a loss of spectral information especially for small features.

2.2.5 Method of Price and Method of Park & Kang

In Price's method it is assumed that a high resolution panchromatic image X and a low resolution multispectral image Y are available [14]. Y_{ij} represents the ij pixel value for low spatial resolution data, and x_{uv} represents the uv pixel value for high resolution data with m the ratio of lengths of sides of the respective pixels. Each low resolution pixel corresponds to m^2 high resolution pixels. Let's make m^2 (also called the magnifying factor) to be 2×2. So each low resolution pixel (i,j) consists of four high resolution pixels (u,v) with

$$(u,v) \in H_{ij} = \{(2i,2j),(2i+1,2j),(2i,2j+1),(2i+1,2j+1)\}.$$

The performance of this method was investigated in using two sets of 500×500 Landsat 7 Enhanced Thematic Mapper (ETM)+ panchromatic (15m resolution) and multispectral (seven bands and 30m resolution except for the thermal band, which is 60m resolution) images. Its performance over IHS and Prices methods was confirmed visually and quantitatively. It was shown that incorporating several high resolution images makes a further improvement to the quality of the result. But the method may not provide a radiometrically accurate fusion if there is a large number of mixed pixels in the low resolution image. In addition, the proposed algorithm needs much processing time for calculating spatially adaptive weights.

2.2.6 The Bayesian methods

Bayesian theory has an important application in statistical modeling. The two main components that make up the Bayesian theory are the prior information and the conditional information in order to get a better estimate called a *maximum a posteriori (MAP)* result. Two methods of super resolution and pan-sharpening of multispectral images, Method of Eismann et al [28], and Method of Molina et al [32], that are done under the Bayesian framework will be discussed here as the models in this research are put under Bayesian formulation.

Method of Hardie and Eismann et al

In this method a *maximum a posteriori (MAP)* estimation method is developed for enhancing the spatial resolution of a hyperspectral image using a higher resolution coincident panchromatic image [28]. The panchromatic high resolution image x can be written as:

$$x = S^t y + \eta \tag{2.4}$$

where y is the high resolution multispectral image to be estimated, S^t is a sparse matrix whose rows are the spectral response functions for the panchromatic pixel locations and η is the noise. Equation 2.4 produces $P(x|y)$.

The low resolution observations Y can be expressed as:

$$Y = Hy + \varepsilon \tag{2.5}$$

where ε is the noise and H is a sparse matrix whose rows are the spatial response functions for the low resolution hyperspectral pixels. Equation 2.5 produces $P(Y|y)$.

Using the Bayesian paradigm, the goal was to find the *maximum a posteriori (MAP)*, that is

$$\hat{y} = argmax_y P(y|x, Y), \tag{2.6}$$

where $P(y|x, Y) \propto P(y)P(x, Y|y)$

Assuming independence between x and Y given y,

$$P(y|x, Y) \propto P(y)P(x|y)P(Y|y)$$

or $P(y|x, Y) \propto P(y|x)P(Y|y)$

Now the remaining task is the definition of $P(y)$ or the conditional distribution $P(y|x)$ depending on the model they want to use.

Using the model

$$P(y|x,Y) \propto P(y)P(x|y)P(Y|y)$$

the authors propose to estimate $P(y,x)$ using a joint Gaussian distribution for (y,x) and then calculate the conditional. Mean and covariance matrices are obtained from the panchromatic and low resolution images. Covariance matrices are improved by the use of clustering techniques.

Using the model

$$P(y|x,Y) \propto P(y)P(x|y)P(Y|y)$$

they estimated $P(y)$ for each pixel as a mixture of Gaussian distributions and the mean and covariance of each member of the mixture is estimated using the Stochastic Mixing Model (SMM). The element of the mixture with the highest probability defines then the prior model.

The method was tested on three types of images: the first was a synthetically generated image that provide a well-controlled test case where the imagery is known to conform to the basic model assumption. The second image was collected by the Airborne Visible-In-frared Imaging Spectrometer (AVIRIS) sensor. The third image was collected by the NVIS airborne sensor which is a pushbroom dispersive imaging sensor. The results showed that better hyperspectral resolution enhancement results than conventional methods such as principal component substitution and least square estimation can be obtained using the method.

Method of Molina et al

Another method of pan-sharpening called, the new super resolution Bayesian method for pan-sharpening Landsat ETM + imagery, constructs the multispectral image y from its corresponding observed low resolution multispectral image $Y$and the high resolution panchromatic image x by using a linear combination of the high resolution multispectral bands, y^b, to obtain the information that is contained in the panchromatic image [32]. i.e.

$$x = \sum_b \lambda^b y^b + \rho, \tag{2.7}$$

where $\lambda^b > 0$ are quantities that are used to weight the contribution of each high spatial resolution multispectral band to the pan image and ρ is the observation noise assumed to be Gaussian with mean equal to zero and variance $1/\gamma$.

In addition, the equation

$$Y^b = H^b y_i^b + \eta^b, \tag{2.8}$$

where H^b is a matrix used to reproduce the low resolution band from the reconstructed high resolution band and η^b is the observation noise assumed to be

Gaussian with mean zero and variance $1/\beta^b$.

Prior model about the smoothness of the object with in each band was modeled using

$$P(y) = \textit{const} \times \prod_b exp\{\frac{-1}{2}\alpha^b \|Cy^b\|^2\} \tag{2.9}$$

where *const* is a constant, C denotes the Laplacian operator, and α^b is the inverse of the variance of the Gaussian distribution.

Given the degradation model for the PAN image in equation 2.7, the distribution of the panchromatic image x given y is defined by

$$P(x|y) = \textit{const} \times exp\{\frac{-1}{2}\gamma \|x - \sum_b \lambda^b y^b\|^2\} \tag{2.10}$$

From the degradation model described in equation 2.8 the distribution of the observed multispectral image Y given y is defined by

$$P(Y|y) = \textit{const} \times \prod_b exp\{\frac{-1}{2}\beta^b \|Y^b - H^b y^b\|^2\} \tag{2.11}$$

The true y is based on $P(y|Y,x)$ given by

$$P(y|Y,x) \propto P(y)P(Y|y)P(x|y) \tag{2.12}$$

Maximization of this equation with respect to y yields the *maximum a posteriori (MAP)* estimate of y. Substituting equations 2.9, 2.10, 2.11 in 2.12 and maximizing with respect to y^b one can obtain,

$$\hat{y^b} = argmin_{y^b} \alpha^b \|Cy^b\|^2 + \beta^b \|Y^b - H^b y^b\|^2 + \gamma \|x - \lambda^b y^b - \sum_{j \in \bar{y^b}} \lambda^j y^j\|^2, \tag{2.13}$$

where $\bar{y^b}$ represents the rest of the bands except y^b. Minimization of the equation is carried out by the following iterative gradient descendent algorithm.

$y^b_{i+1} = y^b_i -$

$$\varphi\{\alpha^b C^t C y^b_i - \beta^b H^{b^t}(Y^b - H^b y^b_i) - \gamma\lambda^b(x - \lambda^b y^b_i - \sum_j \in \bar{b}\lambda^j y^j)\}, \tag{2.14}$$

where y^b_{i+1} and y^b_i are the high resolution estimates of the band b at the $(i+1)^{th}$ and i^{st} iteration steps respectively and φ is the relaxation parameter that controls the convergence of the algorithm. Minimization was done with respect to each band in a cyclic fashion; that is, for each iteration of the algorithm each band is optimized while keeping the rest of the bands fixed. The method developed gives a good result for Landsat 7 ETM and multispectral bands in preserving the spectral information and increasing the spatial resolution.

2.2.7 Summary

Having reviewed the well known methods for image pan-sharpening the focus of this research is to develop a new Bayesian pan-sharpening method using the Markov Random Field (MRF) and the simulated annealing algorithm for satellite images that gives a *maximum a posteriori (MAP)* estimate of the pan-sharpened image. The method developed in this research is similar to the method of Molina et al. [32]. Their method is an MRF-deterministic method where optimization is carried out by gradient-descent optimization procedure that leads to locally optimal solution that does not correspond to *MAP* solution. The MRF and SA-based method developed in this study is an MRF-stochastic method which is non-deterministic, and any next value is determined by randomness and partially but not fully determined by the previous value. The random assignment is based on the Gibbs sampler. The prior model of the method is not based on a quadratic potential function like their method; rather an exponential based potential function is used. In addition optimization is done in such a way that global minimization can be carried out without keeping any other band constant. Chapter 4 discusses the method in a more detailed manner.

Chapter 3

Data and pre-processing

This chapter discusses about the data sets that are used in the research including the preprocessing steps and the degradation procedures. In this research three types of remote sensing data - IKONOS & QuickBird images and an aerial photograph - and two types of synthetic data are used. Section 3.1 discusses about the generation of the synthetic data and its degradation procedures. Section 3.2 discusses about the remote sensing data set in brief.

3.1 Synthetic data sets

Many researches reveal the use of synthetic data as a useful source of data for improving and testing the performance of spatial and spectral multi-resolution image fusion techniques. They are used to improve our understanding of information extraction from remotely sensed data [33, 37]. The main advantage of using a synthetic image in this research is that the exact values of targeted pan-sharpened image will be known. Besides since these synthetic images represent simple geometric features a visual checking of the method's performance will be easier. At the same time a good reference image that will be used to compare with the pan-sharpened image is not available, so the synthetic image can be used to make a quick visual comparison with a reference data. Unlike that of synthetic data, for real data it is almost difficult to get a high resolution multispectral image having the same spatial resolution as that of the pan-sharpened image from sensors. For these reasons two types of synthetic data are prepared.

3.1.1 Synthetic data I

A synthetic pan-sharpened image is generated having four different bands. The pixel values are assigned randomly in such a way that geometric features can easily be checked visually. Figure 3.1 shows the synthetic pan-sharpened image prepared.

Image degradation model

From the prepared synthetic pan-sharpened image two synthetic images one multispectral (four bands) and another panchromatic images are degraded.

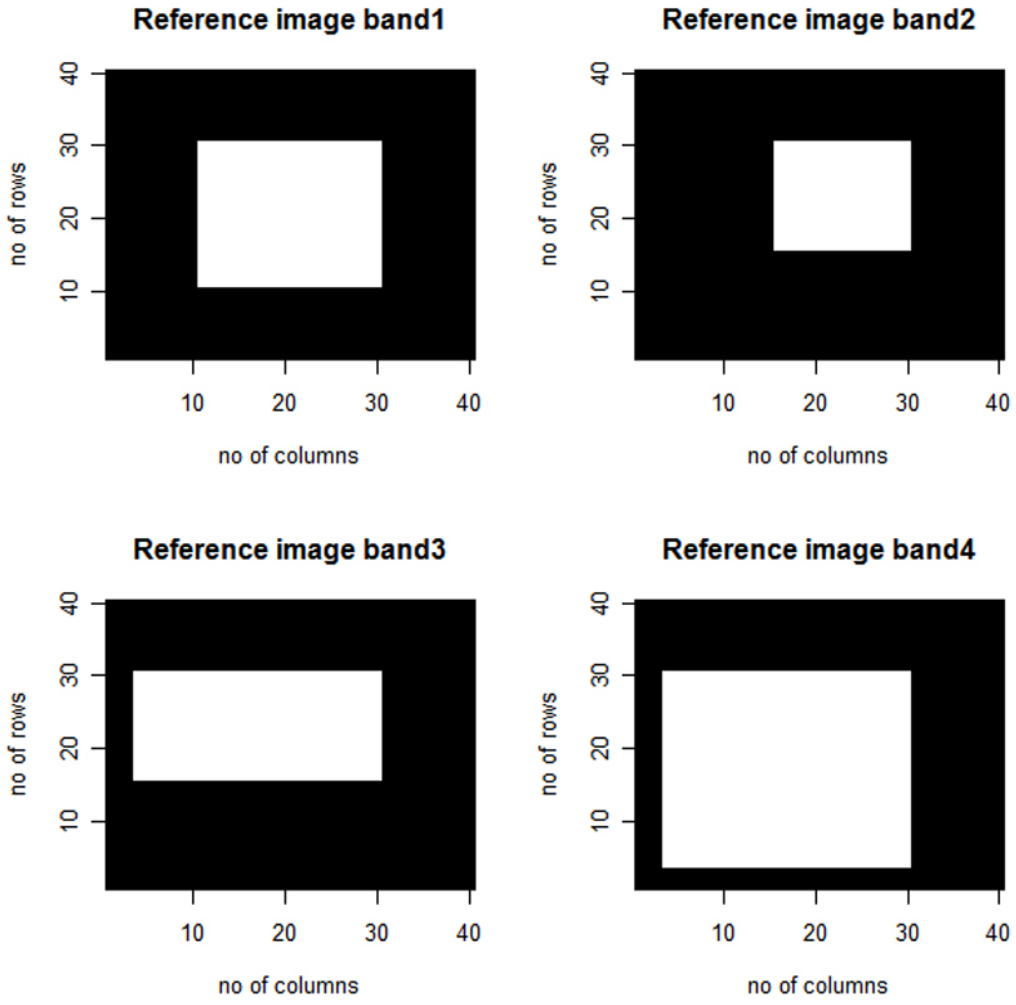

Figure 3.1: *A synthetic pan-sharpened (assumed) image of size* 40×40 *pixel.*

The synthetic pan-sharpened image, the degraded multispectral image and degraded panchromatic image are denoted by F, D and P respectively. The multispectral image is of spatial resolution r and the panchromatic image is of spatial resolution R, where the scale factor S between the two input images is $S = \frac{R}{r}$. If $S = 4$ and (u, v) denotes the pixel of the multispectral image D then this pixel consists of sixteen high resolution pixels (i, j) of the pan-sharpened image F. Where

$$\begin{aligned}(i,j) \in H_{uv} = \{&(4u-3,4v-3),(4u-3,4v-2),(4u-3,4v-1),(4u-3,4v),\\ &(4u-2,4v-3),(4u-2,4v-2),(4u-2,4v-1),(4u-2,4v),\\ &(4u-1,4v-3),(4u-1,4v-2),(4u-1,4v-1),(4u-1,4v),\\ &(4u,4v-3),(4u,4v-2),(4u,4v-1),(4u,4v)\}.\end{aligned}$$

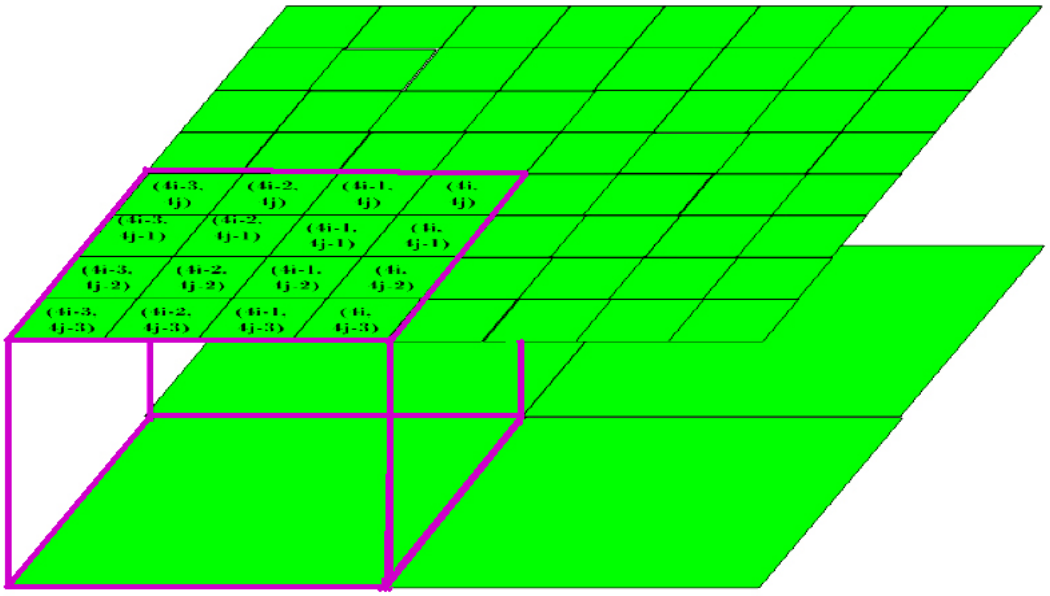

Figure 3.2: *A band of the high resolution image that we want to estimate (upper) and a band of the observed low resolution image (lower).*

Since the scale factor of the images is 4 the following linear relationship model to degrade the synthetic multispectral image from the synthetic pan-sharpened image is used.

$$D^b(u,v) = \frac{1}{16} \sum_{(i,j)\in H_{uv}} F^b(i,j) + \eta^b, \tag{3.1}$$

where D^b is the degraded multispectral image band, F^b is the synthetic pan-sharpened image band and η^b is the observation noise assumed to be Gaussian with mean zero and variance $\frac{1}{\beta^b}$. A brief illustration of the above relationship between the assumed pan-sharpened image and the multispectral image is given in figure 3.2.

Table 3.1: *Assumed values for parameters in the degradation process*

Parameter	η^b	β^b	ρ	γ	ω^b
Value	0	1	0	2	0.25

In addition a synthetic panchromatic image is also degraded from the synthetic pan-sharpened image using the following linear relationship model.

$$P = \sum_b \omega^b F^b + \rho, \tag{3.2}$$

where ω^b are values that weight the contribution of each band of the pan-sharpened image to the panchromatic image and ρ is the observation noise

assumed to be Gaussian with mean zero and variance $\frac{1}{\gamma}$. The weights ω^b are assigned a value of 1 for each band. Figure 3.3 shows the degraded multispectral and panchromatic image bands. Table 3.1 gives the assumed parameter values in the degradation process of both the multispectral and the panchromatic images.

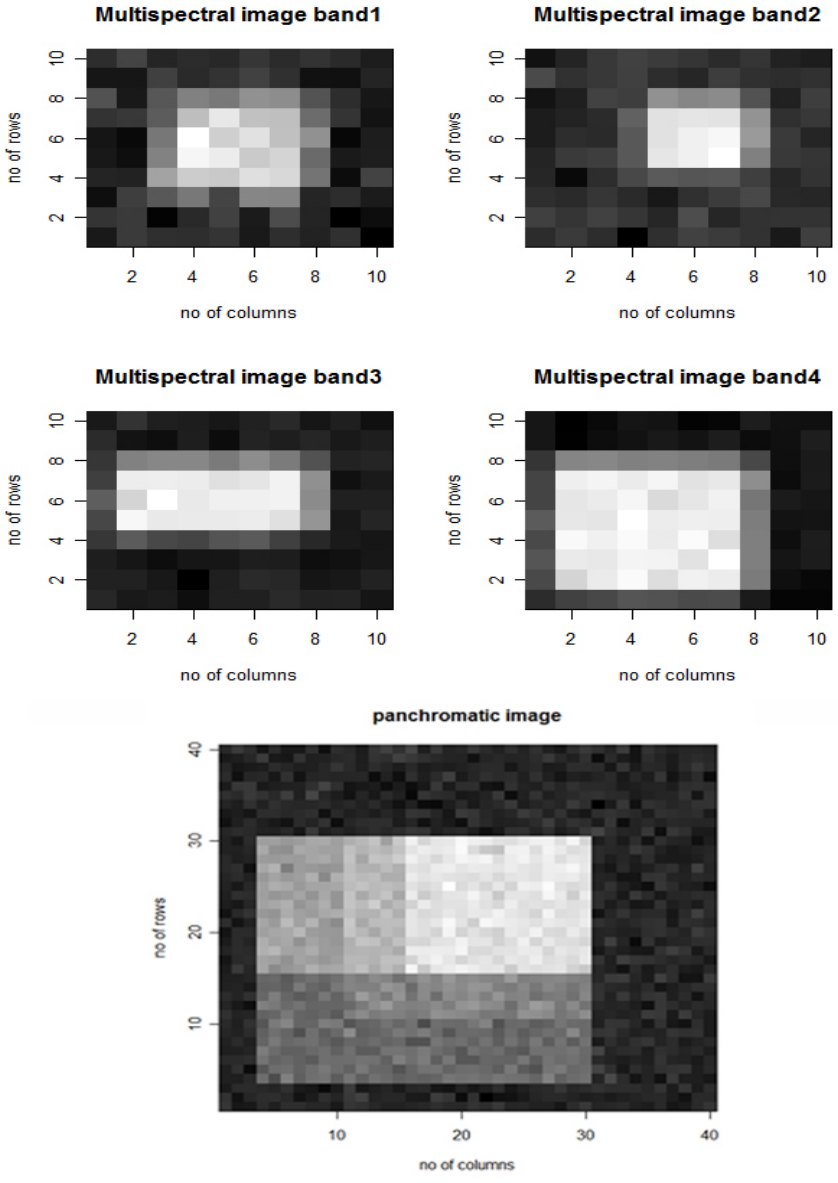

Figure 3.3: *Degraded synthetic multispectral* (10×10 *pixel) and panchromatic* (40×40 *pixel) images.*

3.1.2 Synthetic data II (from IKONOS image)

The IKONOS Satellite, launched on 24 September 1999 in Vandenberg Air Force Base, California, USA, is a high-resolution satellite operated by GeoEye. It can capture a 3.2m multispectral and a 0.82m panchromatic resolution images at nadir, and a 4.0m multispectral and a 1.0m panchromatic images at 26 degree off nadir. IKONOS data is collected as 11 bits per pixel. Since it has both cross and along track viewing instruments flexible data acquisitions and frequent revisiting are possible. It can yield relevant data for nearly all aspects of environmental study [6]. Table 3.2 summarizes the detail technical information of the satellite imagery.

Table 3.2: *Technical details of IKONOS satellite*

Band Name	*Wave length (nm)*	*Resolution off-nadir(m)*	*Swath width (km)*	*Revisit time(days)*
Pan	525.8 -928.5	1	11.3	3
MS-1 (Blue)	444.7 -516.0	4	11.3	3
MS-2 (Green)	506.4- 595.0	4	11.3	3
MS-3 (Red)	631.9 -697.7	4	11.3	3
MS-4 (VNIR)	757.3- 852.7	4	11.3	3

Figure 3.4 shows the spectral response curve for the different bands of the satellite imagery. It shows that the spectral response of the pan is not uniform in the entire wavelength; it is very low in the blue band and maximum in the Green, Red and NIR bands and extends beyond 0.90m.

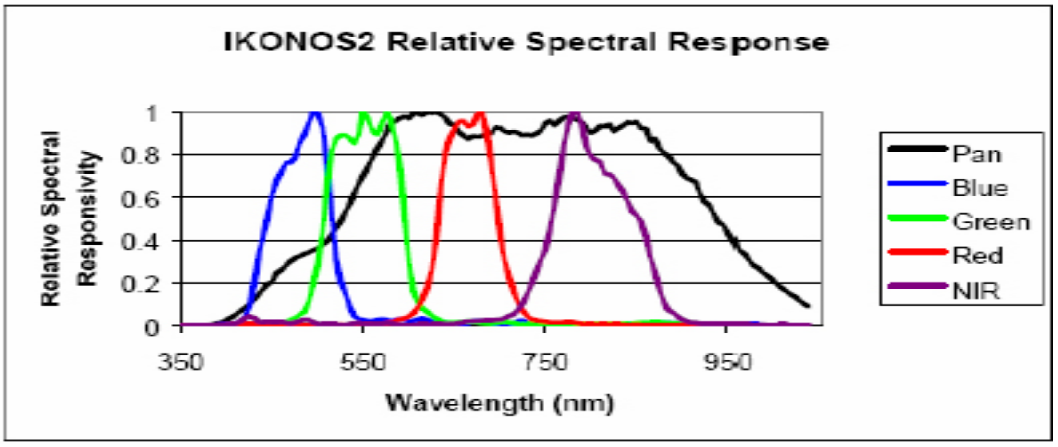

Figure 3.4: *Spectral response curve of IKONOS imagery* (Source: NASA Library).

In this study part of the IKONOS image of the Enschede area, The Netherlands, obtained in April 2000 is used. The multispectral image used is 4 meter resolution and the panchromatic image is 1 meter resolution. A synthetic data is prepared using the multispectral IKONOS image. Figure 3.5 shows the subset of both the multispectral and the panchromatic images used for this study.

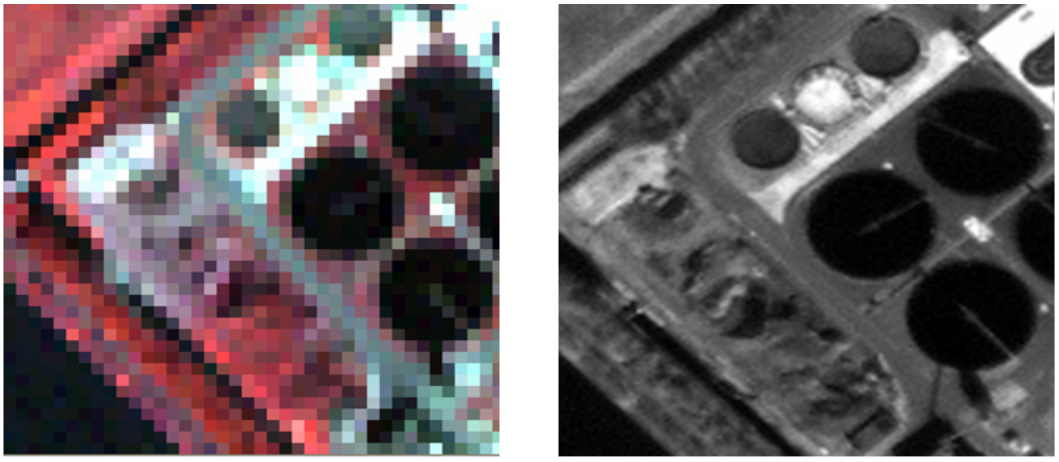

Figure 3.5: *Subset of IKONOS multispectral (left) and panchromatic (right) images* .

Preprocessing and Image degradation

Various preprocessing steps should be done before performing sharpening on a set of images. Co-registration, viewing angle of the imagery and resampling methods used for geometric correction and projection are the main factors that should be considered [16, 23]. The multispectral and the IKONOS images that are used for this study are already co-registered with the same Map Projection: Universal Transverse Mercator with Datum: WGS84.

Figure 3.6: *Pan-sharpened (assumed), degraded multispectral and panchromatic (from left to right respectively) subset images of IKONOS* .

Since the two images are taken at the same time the viewing angle of the images are the same and pan-sharpening can be done. From the metadata of the image it is understood that a bicubic interpolator method is used as a resampling technique (already by the company that produced the images) and the images are also already standard geometrically corrected.

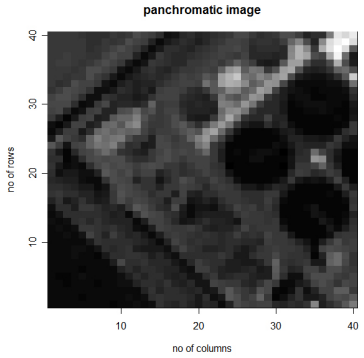

Figure 3.7: *Degraded panchromatic bands of the subset of IKONOS image.*

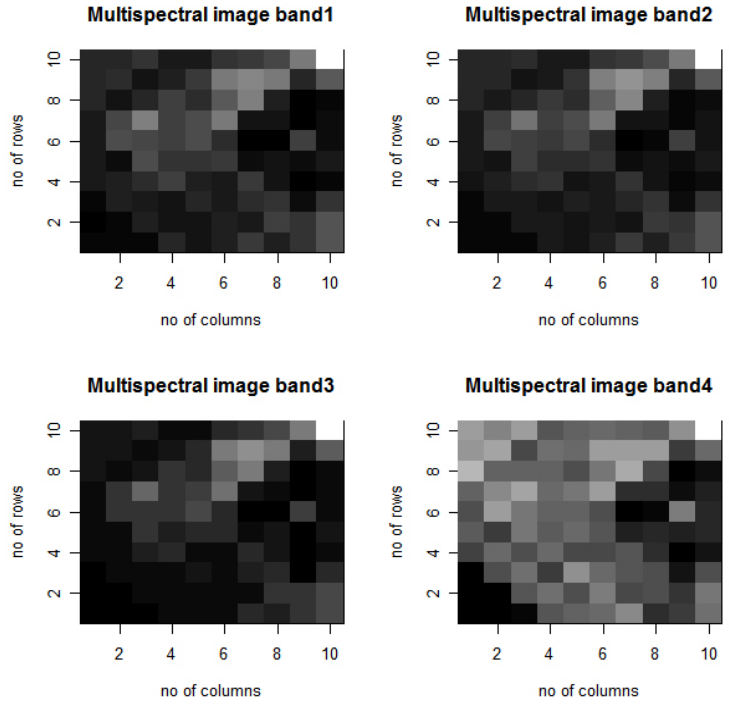

Figure 3.8: *Degraded multispectral bands of the subset of IKONOS image.*

In this research the IKONOS image is used to validate the performance of the method and to do experiments in order to estimate some parameters (to be discussed in chapters 4 and 5). So a small subset (40×40 pixel) of the multispectral

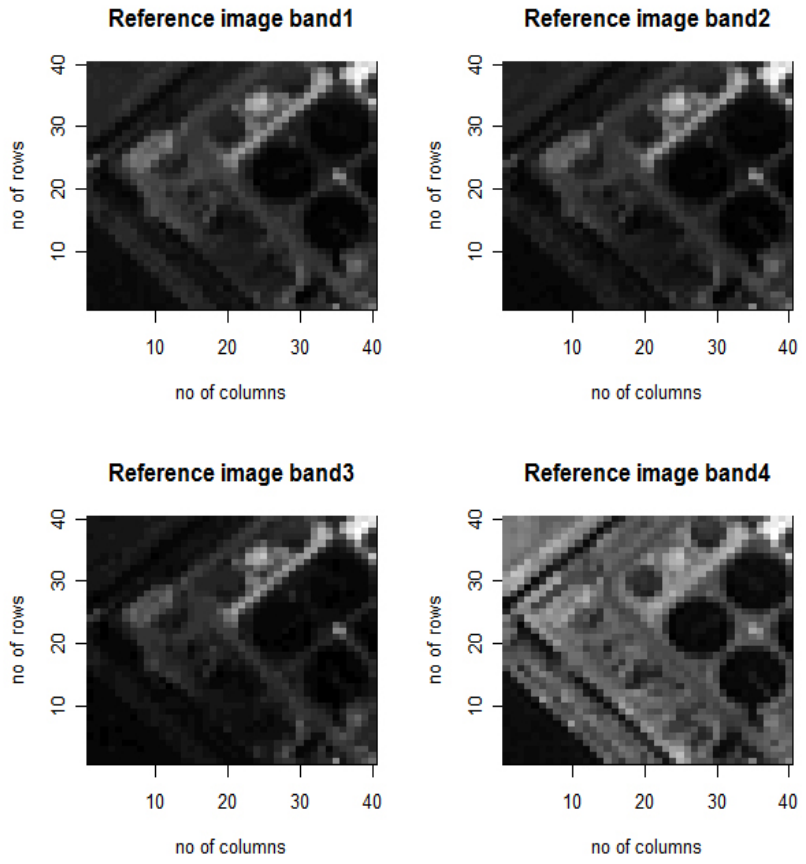

Figure 3.9: *Reference (assumed pan-sharpened) subset bands of IKONOS image.*

image is taken and considered it as a pan-sharpened image and two images one multispectral (degraded spatially) and another panchromatic (degraded spectrally) are degraded out of it. The models used for the degradation procedure are done the same way done for the synthetic image using the equations 3.1 and 3.2. Figure 3.6 shows the assumed pan-sharpened image (the multispectral subset) the degraded multispectral image and the degraded panchromatic image, and Figure 3.7, 3.8 and 3.9 shows the degraded panchromatic image band, the degraded multispectral image bands and the reference image (assumed pan-sharpened) bands respectively.

3.2 Remote sensing data sets

3.2.1 QuickBird image

The QuickBird satellite, launched on 18 October 2001 in Vandenberg Air Force Base, California, USA is a high-resolution satellite operated by DigitalGlobe. It offers highly accurate, commercial high-resolution imagery of Earth. It can capture a 2.44 multispectral and a 61 cm panchromatic resolution images at

nadir, and a 2.88 m multispectral and a 72 cm panchromatic image at 25 degree off nadir. QuickBird data is collected as 11 bits per pixel. Like that of IKONOS image it has both cross and along track viewing instruments so that flexible data acquisitions and frequent revisiting are possible. The satellite is an excellent source of environmental data useful for analysis of changes in land usage, agricultural and forest climates and it yield relevant data for almost all aspects of environmental study [4]. Table 3.3 summarizes the detail technical information of the satellite imagery.

Table 3.3: *Technical details of QuickBird satellite*

Band Name	*Wave length (nm)*	*Resolution off-nadir(m)*	*Swath width (km)*	*Revisit time(days)*
Pan	450 - 900	0.72	16.5	1 - 3.5
MS-1 (Blue)	450 - 520	2.88	16.5	1 - 3.5
MS-2 (Green)	520 - 600	2.88	16.5	1 - 3.5
MS-3 (Red)	630 - 690	2.88	16.5	1 - 3.5
MS-4 (VNIR)	760 - 900	2.88	16.5	1 - 3.5

Figure 3.10 shows the spectral response curve for the different bands of the satellite imagery. It shows that the sensor has low spectral response in the Blue band, and maximum in the Green-Red bands. It also shows that though the spectral ranges of the Pan sensors are provided as 0.45-0.90 m, the spectral sensitivity is not uniform over the MS bands.

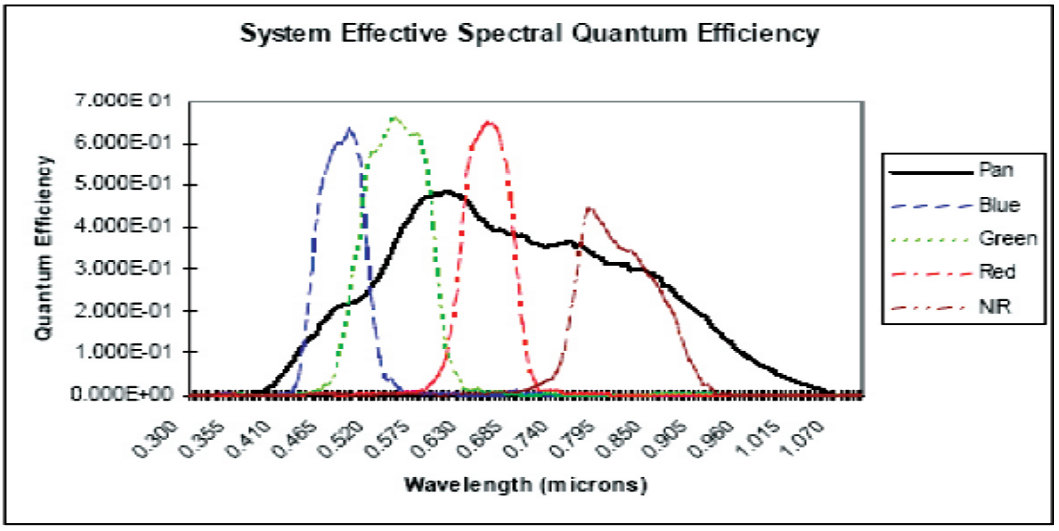

Figure 3.10: *Spectral response curve of QuickBird imagery* (Source: NASA Library).

In this study part of the QuickBird image of the Enschede area, The Netherlands, obtained in September 2006 is used. Like that of the IKONOS image the multispectral image used is 4 meter resolution and the panchromatic image is 1 meter resolution. Figure 3.11 shows a 120×120 pixel subset of the panchromatic image of Enschede area and a corresponding 30×30 pixel subset of the multispectral image of the same area (4,3,2 band combination). In this research this larger subset of QuickBird image is used to produce a pan-sharpened image to see how the method performs.

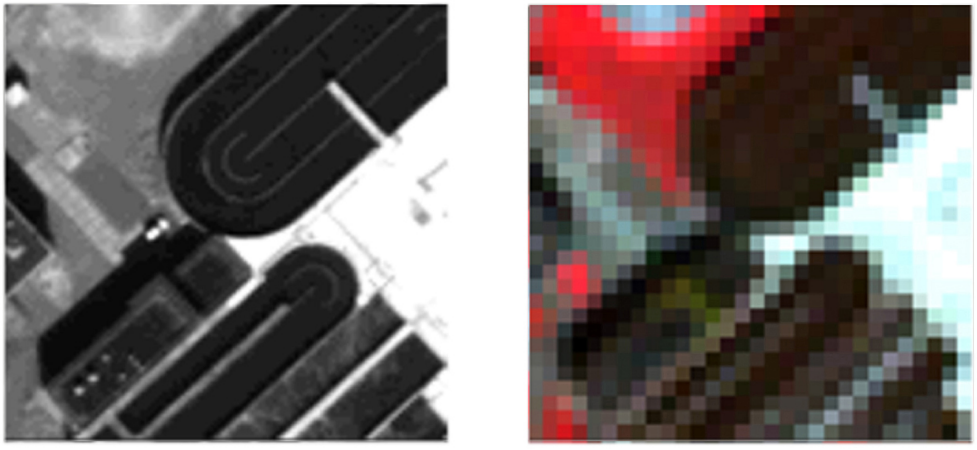

Figure 3.11: *Subset of QuickBird panchromatic image(left) and multispectral image (right).*

As it can be seen from the two figures the multispectral image has a higher spectral information but a lesser spatial resolution than that of the panchromatic image. A pan-sharpened image that has better spectral resolution than the panchromatic image and better spatial resolution than the multispectral image is expected to have using the method.

Preprocessing

It is understood that various preprocessing steps should be done before performing sharpening on a set of images like Co-registration, viewing angle of the imagery and resampling methods used for geometric correction and projection. The multispectral and the IKONOS images that are used in this study are already co-registered with the same Map Projection: Universal Transverse Mercator with Datum: WGS84. Since the two images are also taken at the same time the viewing angle of the images are the same and pan-sharpening can be done. From the metadata of the image it is understood that the images are already standard geometrically corrected.

3.2.2 Aerial Photograph

A subset of an airborne image of the same area is also taken as one part of the data to be used in this study. The image is taken on March 30, 1998 and

Figure 3.12: *Subset of aerial image.*

has a spatial resolution of 1 meter. Figure 3.12 shows a subset of the aerial photograph. In addition to the other methods of assessing the result of the research, a visual comparison between this aerial image and the pan-sharpened image will be done to assess the accuracy of the final pan-sharpened image. Detail explanation on the accuracy assessment is given in the last sections of chapter five.

Chapter 4

MRF & simulated annealing-based pan-sharpening method

This chapter introduces the technique of MRF & simulated annealing-based pan-sharpening which is employed in this research. The first section, section 4.1 briefly discusses about a neighborhood system and the MRF and the Gibbs random fields. Section 4.2 and 4.3 illustrates how the prior and the conditional energies are modeled respectively. Section 4.4 discusses how the global energy is constructed and optimized. Lastly section 4.5 explains how the method is assessed. All the processing and computation is done using the R programming language and environment for statistical computation, version 2.4.0 [3]. The main references for the coming sections are [24, 26], the interested reader can refer to them for more detail.

4.1 Neighborhood system and MRF & Gibbs random fields

4.1.1 Neighborhood system

Consider a rectangular fine resolution image of size $M \times N$ and $d = \{d_1, d_2, ..., d_m\}$ denotes a set of pixels. We say the pixels in d are related to one another via a neighborhood system. A neighborhood system for d is defined as:

$$N = \{N_i | \forall i \in d\}, \tag{4.1}$$

where N_i is the set of pixels neighboring pixel i. Two properties are there for a neighborhood system.

1. $i \notin N_i$, a pixel can not be a neighbor to itself
2. $j \in N_i \Leftrightarrow i \in N_j$, the neighboring relationship is mutual

A popular choice for neighborhood system in image analysis is the first-order neighbors as the four pixels that share a side with a given pixel which is as

shown in figure 4.1(a). Second-order neighbors are the four pixels having corner boundaries with a given pixel as shown in figure 4.1(b); and higher-order, for instance, fifth order neighbors can also be extended like wise as shown in figure 4.1(c). Even though it is possible to use different neighborhood order it is stated in most literature that a neighborhood order of two is sufficient [24, 26]. In this study the neighborhood order is proposed in relation to the scale factor [33]. The scale factor between the multispectral and the panchromatic image is 4. So all pixels present within the coarse multispectral image pixel can be included in the neighborhood system and this enables to keep the locality property within the neighboring pixels [18]. A neighborhood size of various window size is used. The minimum neighborhood order considered is first-order or window size 1. In some literature [33] the following relation is also used to determine the window size (W_{size}) of a neighborhood system.

$$W_{size} = 2 * S - 1 \tag{4.2}$$

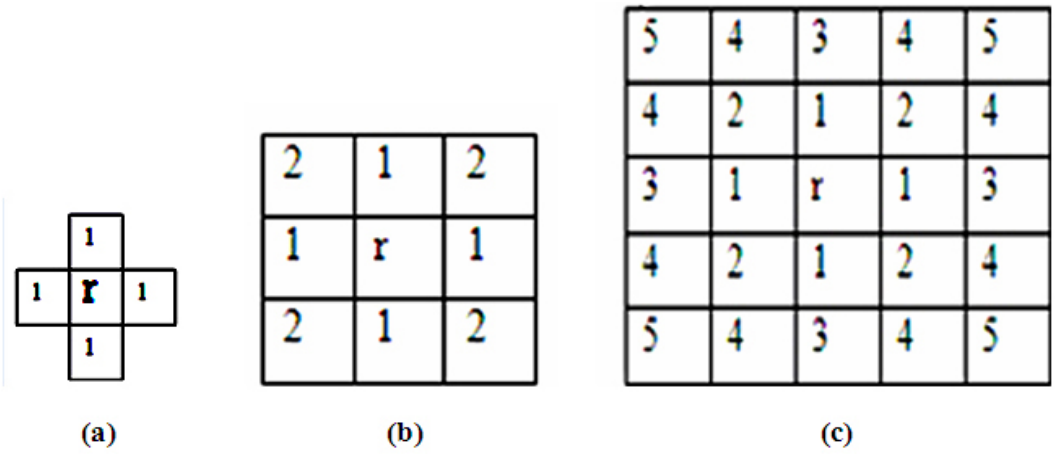

Figure 4.1: *Neighborhood order for a pixel r.(a),(b),(c) shows the first, second and fifth order neighborhood system, respectively (adapted from (26)).*

4.1.2 MRF and Gibbs random fields

Suppose d denotes a set of random variables $d = \{d_1, d_2, d_3, ..., d_m\}$ and is defined on a set A that contains m number of sites. The family d is called a random field. We can consider the set A as an image containing m pixels, then in this case d will be a set of pixel DN values. Now based on this random field let's consider a set F for the set A as $F = \{d_1 = F_1, d_2 = F_2, d_3 = F_3, ..., d_m = F_m\}$ which will be denoted as $F = \{F_1, F_2, F_3, ..., F_m\}$. A random field with respect to a neighborhood system is called a Markov random field if the probability density function satisfies the following three properties.

1. Positivity: $P(F) > 0$ for all possible configurations of F,

2. Markovianity: $P(F_r \mid F_{A-r}) = P(F_r \mid F_{Nr})$, where $r \in 1, .., m, \quad A - r$ are all pixels in the set excluding r, F_{A-r} denotes the set of labels at the sites in $A - r$, N_r denotes the neighbors of r and,

3. Homogeneity: $P(F_r \mid F_{Nr})$ is the same $\forall$ sites r

The first property is usually true in practice. The basic idea behind the second and the third mathematical properties is that, the second one states that the probability of a certain pixel is only dependent on its neighbors. The third one states that the conditional probability of a certain pixel with respect to its neighbors is the same as the conditional probability of the pixel with all of the pixels excluding the pixel itself.

If an energy function $U(F)$ can be expressed as,

$$U(F) = \sum_{c \in C} V_c(F) \tag{4.3}$$

where C is called a *clique* which is a collection of all possible cliques (a clique is but a subset of F in which all pairs of sites are mutual neighbors. It can be a single site, a pair of neighbors site, or a triple of neighboring sites, etc.) and $V_c(F)$ called the potential function with respect to clique type C, then a Gibbs random field (GRF) can give a global model for an image specifying the following form of probability density function,

$$P(F) = \frac{1}{Z} \exp[-\frac{U(F)}{T}] \tag{4.4}$$

where F is as defined above, T is a constant termed temperature (mostly equal to 1), and Z is called the partition function which is a normalizing constant expressed as,

$$Z = \sum_{F} \exp[-\frac{U(F)}{T}] \tag{4.5}$$

Since Z is the sum of all configurations of F, it is mostly difficult to calculate Z and is usually set to be equal to 1. From equation 4.4 it follows that maximizing $P(F)$ is equivalent to minimizing the energy function $U(F)$.

Note that Gibbs random field and Markov random field are equivalent as far as the cliques are concerned. One can read the conceptual and the mathematical proof in the book by [26] where most of the above basic ideas of MRF are well explained.

In this study the terms prior (conditional) information and prior (conditional) energy can be used interchangeably. But energy and probability have inverse relationships. Minimum energy implies maximum probability and vise versa.

4.2 Modeling prior energy

This section briefly describes how a model for prior energy is constructed using the MRF. The choice of the form and the parameters of a function for the energy function $U(F)$ is an important topic in MRF modeling. A pair wise clique (window size of one) potential function is reported to be sufficient for a variety of image analysis applications [24] that allows the following expression.

$$U(F) = b \sum_{\{r,r'\} \in C_2} V(F_r, F_{r'}) \tag{4.6}$$

which can be rewritten as,

$$U(F) = b \sum_{\{r,r'\} \in C_2} (F_r - F_{r'})^2 \tag{4.7}$$

where b is a potential parameter, V is a potential, r is a pixel and r' is a neighborhood pixel and C_2 is the set containing pairwise pixels. In this study the prior energy is modeled as follows:

$$U_{prior}(F_i) = \sum_b \alpha_b \sum_{j \in N_i} W_j \; g(F_i^b - F_j^b) \tag{4.8}$$

where,

$$g(x) = \rho(1 - \exp \frac{-x^2}{\rho}) \tag{4.9}$$

where $g(x)$ is the potential function for the discontinuity adaptive (DA) MRF model (this form of potential function is chosen in order to smooth differences between pixel values smaller than ρ), b represents, α_b are the relevance of the different bands for the prior energy, F_i^b is value of pixel i of band b of pan-sharpened image F, F_j^b shows the neighborhood pixel j of band b of image F, and W_j is the weight given to the contribution of the neighborhood pixel calculated as,

$$W_j = \frac{Const}{\sum_{j=1}^{N_i} {d_j}^2} \tag{4.10}$$

where d_j is the distance between pixel i and its neighborhood pixel j expressed in pixel resolution units R, and the $Const$ is chosen so that $\sum_j W_j = 1$.

4.3 Modeling conditional energies

4.3.1 Conditional energy from the panchromatic image

The conditional energy from the panchromatic image is modeled using the probability density function defined by Alvarez et al. [9] used to obtain high resolution images from a sequence of low resolution images that are acquired by a

single sensor imaging the scene over a period of time. The panchromatic image is obtained using the degradation model discussed in section 3.1.1. The assumed relation ship between the panchromatic image and the pan sharpened image is as follows:

$$P_i = \sum \omega^b F_i^b + \rho_i \tag{4.11}$$

The conditional probability of the panchromatic image based on the pan sharpened image is given as,

$$P(P_i|F_i) = const \times exp\{\frac{-1}{2}\gamma(P_i - \sum_b \omega^b F_i^b)^2\} \tag{4.12}$$

where P is the panchromatic image, F is the pan-sharpened image, ω^b denotes the weight given to the contribution of the pan-sharpened image bands to the panchromatic image, ρ is the observation noise assumed to be Gaussian with mean equal to zero and variance $\frac{1}{\gamma}$.

From the relationship between probability and energy the above probability density function provides the following conditional energy equation.

$$U(P_i|F_i) = const + \frac{1}{2}\gamma(P_i - \sum_b \omega^b F_i^b)^2 \tag{4.13}$$

Since a minimum energy is needed $\frac{1}{2}\gamma$ is incorporated in γ. So the conditional energy of the panchromatic image based on the pan-sharpened image is simplified to the following form in order to get minimum energy.

$$U(P_i|F_i) = \gamma(P_i - \sum_b \omega^b F_i^b)^2 \tag{4.14}$$

4.3.2 Conditional energy from the multispectral image

To model the conditional energy from the multispectral image a model developed by Alvarez et al. [9]is modified. The multispectral image is obtained using the degradation model discussed in section 3.1.1. They assumed the following relationship between the multispectral image and the pan-sharpened image.

$$D_i^b = H^b F_i^b + \eta_i^b \tag{4.15}$$

where H^b is an integration and decimation operator designed to produce the measured low resolution multispectral image, D is the multispectral image defined on coarse resolution pixel grid, and η is a Gaussian noise.

In this study since the scale factor between the multispectral and the panchromatic (hence the pan-sharpened) image is 4, the same to the degradation model as illustrated in figure 3.2 if (u, v) denotes the pixel of the multispectral image D then this pixel consists of sixteen high resolution pixels (i, j) of the pan-sharpened image F. For example if $S = 4$,

$$(i,j) \in H_{uv} = \{(4u-3,4v-3),(4u-3,4v-2),(4u-3,4v-1),(4u-3,4v),\\ (4i-2,4v-3),(4u-2,4v-2),(4u-2,4v-1),(4u-2,4v),\\ (4u-1,4v-3),(4u-1,4v-2),(4u-1,4v-1),(4u-1,4v),\\ (4u,4v-3),(4u,4v-2),(4u,4v-1),(4u,4v)\}.$$

So the above linear relationship model is modified as follows,

$$D^b(u,v) = \frac{1}{S^2} \sum_{(u,v)\in H_{ij}} F^b(i,j) + \eta^b \tag{4.16}$$

where D^b is the multispectral image band, F^b is the pan-sharpened image band and η^b is the observation noise assumed to be Gaussian with mean zero and variance $\frac{1}{\beta}$.

The conditional probability of the panchromatic image based on the pan sharpened image is given as,

$$P(D_i|F_i) = const \times \prod_b exp\{\frac{-1}{2}\beta^b(D_i^b - H^b F_i^b)^2\} \tag{4.17}$$

From the relationship between probability and energy the above probability density function provides the following conditional energy equation.

$$U(D_i|F_i) = const + \sum_b \frac{1}{2}\beta^b(D_i^b - H^b F_i^b)^2 \tag{4.18}$$

Since the interest is to find F that minimizes the energy U, $\frac{1}{2}\beta^b$ is incorporated in β^b. So the conditional energy of the multispectral image based on the pan-sharpened image is simplified to the following form in order to get minimum energy.

$$U(D_i|F_i) = \sum_b \beta^b(D_i^b - H^b F_i^b)^2 \tag{4.19}$$

4.4 Global energy Construction and optimization

To get the MAP estimate the posterior probability for image F has to be maximized. In other words the total energy has to be minimized. Three energy models: *a priori* energy (U_{prior}), a conditional energy from the panchromatic image ($U(P_i|F_i)$) and a conditional energy from the multispectral image ($U(D_i|F_i)$) are developed. These three energies are considered under Bayesian context to get the minimum energy.

According to Bayes formula for two events a and b:

$$P(a|b) \propto \frac{P(b|a)P(a)}{\sum P(a|b)P(b)} \tag{4.20}$$

In this study since there are two conditional probabilities, equation 4.20 will have the following form:

$$P(F_i|P_i, D_i) = P(P_i|F_i)P(D_i|F_i)P(F_i) \tag{4.21}$$

From the relationship between probability and energy, equation 4.21 becomes,

$$U(F_i|P_i, D_i) = U(F_i) + U(P_i|F_i) + U(D_i|F_i) \tag{4.22}$$

A new parameter λ, $0 < \lambda < 1$, which is called the smoothness parameter is introduced. It is used as a balancing factor between the prior and the conditional energies.

$U_{(total)} = \lambda U_{(prior)} + (1 - \lambda)[U(P_i|F_i) + U(D_i|F_i)]$,

which implies,

$$\begin{aligned} U(F_i|P_i, D_i) = \lambda \textstyle\sum_b \alpha_b \sum_{j \in N_i} W_j \; g(F_i^b - F_j^b) \; + \\ (1 - \lambda)[\gamma(P_i - \textstyle\sum_b \omega^b F_i^b)^2] \; + \\ (1 - \lambda)[\sum_b \beta^b (D_i^b - H^b F_i^b)^2] \end{aligned} \tag{4.23}$$

where $U(F_i|P_i, D_i)$ represents the total energy, $U_{(total)}$.

The *maximum a posteriori (MAP)* solution for the pan-sharpened image pixel $\hat{F_i^b}$ can be found by minimizing the total energy:

$$\hat{F_i^b} = \arg\min_F \{(U_{(total)}|F_i^b)\} \tag{4.24}$$

4.4.1 Initial pan-sharpened image generation

In this study a small part of the IKONOS image is taken and two images are degraded out of it: one panchromatic image P and another multispectral image D where the degradation procedure is as explained in section 3.1.1. The aim is to get a pan-sharpened image using the prior and conditional models developed above and the simulated annealing algorithm in the Bayesian framework. Still the actual pan sharpened image F is not known before the simulated annealing algorithm that updates using the Gibbs sampler is applied. So at the start an initial pan-sharpened image $F[k, l]$ is generated as:

$$F[k, l] = D[ceiling(k/4), ceiling(l/4)] \tag{4.25}$$

where the *ceiling* function takes a single numeric argument x and returns a numeric vector containing the smallest integers not less than the corresponding elements of x, and k & l are rows and columns respectively.

4.4.2 Simulated annealing algorithm

After the introduction of the smoothness parameter and determination of the total energy, the next step is to find the minimum of the total energy in *MAP* estimate. In order to find the global minimum energy, different algorithms like the Maximum a Posterior Margin *(MPM)* and Simulated Annealing *(SA)* can be found in literature [26]. The *(SA)* algorithm is used as it leads to the *MAP* estimate for the solution.

Simulated annealing was first proposed by Metropolis et.al. to simulate the behavior of particles in the thermal equilibrium. It is a type of stochastic iterative optimization technique which is mainly based on the use of random numbers and probability statistics for the global optimization problem [26, 36]. It generates a new label $F_i'^b$ for each pixel F_i^b based on the prior and conditional energies.

The basic idea of this algorithm is just like introducing a noise to a system and then to shake the search process away from the local minimum and get a global minimum value. The process of optimization is controlled by a temperature parameter T. The SA process is iterative, it starts with $T = T_0$ and at the iteration k

$$T_k = \frac{T_0}{\ln(1+k)}, \tag{4.26}$$

where T_0 is an initial temperature and T_k is any next temperature value at the k^{th} iteration. In this research a faster empiric schedule is used which is given as [24]:

$$T_k = T_{k-1} \times \sigma \tag{4.27}$$

There are two main parameters in the simulated annealing algorithm that control the process of optimization. One is T and the other is σ that controls the rate of temperature decrease. Both are parameters that are mostly estimated experimentally.

The temperature parameter T controls the randomness of the optimization algorithm. High temperature reveals high randomness and vise versa. This indicates that high temperature increases the probability of a pixel $F^b(i,j)$ being replaced by a new label $F'^b(i,j)$. This is because the change in energy is less than 0, large T indicates large $\exp(\frac{\triangle U}{T})$, even though the energy of the new label $F'^b(i,j)$ is higher than that of $F'^b(i,j)$. So the algorithm starts at a high temperature T_0. After the new label $F'^b(i,j)$ converges to equilibrium at the current temperature T, the temperature decreases inline with the aforementioned cooling schedule (i.e. $T_k = T_{k-1} \times \sigma$). Usually T_0 is set to a value between 2 and 4, and $0.8 < \sigma < 1$ [26, 36] . When T reaches to a freezing point any increase of energy can not be accepted. That means no pixel will be updated. In this study the pixel updating is done row wise and the iteration was set to finish if three consecutive energies are the same (if there is no change in pixel labeling

for three consecutive iterations).

4.4.3 Gibbs sampler

The Gibbs sampler generates a sequence of energies for each pixel based on the total energy (that means from the three joint probability distributions). It is applicable when the joint distribution is not known explicitly. Gibbs sampling is particularly well-adapted for sampling the posterior distribution of Bayesian networks as Bayesian networks are typically specified as a collection of conditional and prior distributions [40]. Simulated annealing is a stochastic process. So the Gibbs sampler is used to generate random pixel values and for updating the sample for the pan-sharpened image.

4.4.4 Optimization of the pan-sharpened image with SA & Gibbs sampler

The first and the second partial derivatives of the total energy with respect to pixel values F_i^b in all the bands is taken. Note that the expression for the total energy in equation 4.23 is not quadratic in F_i^b because of the choice for $g(x)$. The sampling for F_i^b is derived in the following way.

$$P(F_i^b) \sim e^{-U(F_i^b|P_i,D_i)} \tag{4.28}$$

The total energy expression in equation 4.24 can be rewritten as:

$$\begin{aligned} U(F_i|P_i,D_i) = \lambda\alpha_b \textstyle\sum_b \sum_{j\in N_i} W_j \; g(F_i^b - F_j^b) \; + \\ (1-\lambda)\gamma(P_i - \textstyle\sum_b \omega^b F_i^b)^2) \; + \\ (1-\lambda)\beta^b(\tfrac{1}{S^2}\textstyle\sum_j \in N_{Si} F_j^b - D_{iS}^b) \end{aligned}$$

where j is a neighborhood pixel of pixel i and N_{Si} is a window containing all the neighborhood pixels j of pixel i.

Substituting equation 4.9 in the above expression for the total energy and taking the partial derivative for the total energy (and hence the pan-sharpened image) with respect to the four bands results in the following expression:

$$\begin{aligned} \tfrac{\partial U(F_i|P_i,D_i)}{\partial F_i^b} = \lambda \;\; \alpha_b \;\; \textstyle\sum_{j\in N_i} W_j \times \;\; 2(F_i^b - F_j^b) \;\; \times \exp(\tfrac{-(F_i^b - F_j^b)^2}{\rho}) \; + \\ 2(1-\lambda) \;\; \gamma(\textstyle\sum_b F_i^b \omega^b - P_i) \;\; \omega^b \; + \\ 2(1-\lambda) \;\; \beta^b(\tfrac{1}{S^2}\textstyle\sum_{j\in iS} F_j^b - D_{iS}^b)\tfrac{1}{S^2} \end{aligned}$$

$$\Rightarrow \qquad \tfrac{\partial U(F_i|P_i,D_i)}{\partial F_i^b} \simeq 2\lambda \;\; \alpha_b \;\; \textstyle\sum_{j\in N_i} W_j * \;\; (F_i^b - F_j^b) \;\; \varphi_{ij} \; +$$

$$2\gamma\ \ (1-\lambda)\ \ \omega^b(\textstyle\sum_b F_i^b\omega^b - P_i)\ \ +$$

$$2(1-\lambda)\ \ \beta^b(\tfrac{1}{S^2}(\tfrac{1}{S^2}\textstyle\sum_{j\in iS} F_j^b - D_{iS}^b)),$$

where $\varphi_{ij} = e^{\frac{-(F_i^b - F_j^b)^2}{\rho}}$ is a non linear factor. It is replaced by an approximate expression:

$$\varphi_{ij} \approx \begin{cases} 1 & \text{if } |F_i^b - F_j^b| << \rho \\ 0 & \text{otherwise} \end{cases}$$

Then

$$\frac{\partial U(F_i|P_i,D_i)}{\partial F_i^b} = 2\lambda\ \ \alpha_b\ \ \textstyle\sum_{j\in N_i} W_j\ \ F_i^b\ \ \varphi_{ij}\ -\ 2\lambda\ \ \alpha_b\ \ \sum_{j\in N_i} W_j\ \ F_j^b\ \ \varphi_{ij}\ +$$

$$2\gamma\ \ (1-\lambda)\ \ \omega^b\ \ [F_i^b\omega^b + \textstyle\sum_{b'\neq b} F_i^b\omega^b - P_i]\ \ +$$

$$2(1-\lambda)\ \ \beta^b\tfrac{1}{S^2}\ \ [\tfrac{1}{S^2}F_i^b + \tfrac{1}{S^2}\textstyle\sum_{j\in iS} F_j^b - D_{iS}^b]$$

And finally,

$$\frac{\partial U(F_i|P_i,D_i)}{\partial F_i^b} = 2F_i^b\ \ [\gamma(1-\lambda)(\omega^b)^2 + \lambda\alpha_b\textstyle\sum_{j\in N_i} W_j\varphi_{ij} + (1-\lambda)\beta^b\tfrac{1}{S^4}]\ \ -$$

$$2\ \ [\gamma\ \ (1-\lambda)\ \ \omega^b\ \ (P_i - \textstyle\sum_{b'\neq b} F_i^bW^{)} + \lambda\alpha_b\textstyle\sum_{j\in N_i} W_j\varphi_{ij}F_j^b\ \ +$$

$$(1-\lambda)\beta^b\tfrac{1}{S^2}(D_{iS}^b - \tfrac{1}{S^2}\textstyle\sum_{j\in iS} F_j^b)]$$

$\frac{\partial U(F_i|P_i,D_i)}{\partial F_i^b}$ has a linear form that can be expressed as,

$$\frac{\partial U(F_i|P_i,D_i)}{\partial F_i^b} = 2F_i^b a_1\ \ - 2a_0, \tag{4.29}$$

where

$$a_0 = \gamma\ \ (1-\lambda)\ \ \omega^b\ \ (P_i - \textstyle\sum_{b'\neq b} F_i^bW^{)} + \lambda\alpha_b\textstyle\sum_{j\in N_i} W_j\varphi_{ij}F_j^b\ \ +$$

$$(1-\lambda)\beta^b\tfrac{1}{S^2}(D_{iS}^b - \tfrac{1}{S^2}\textstyle\sum_{j\in iS} F_j^b)$$

$$a_1 \approx \gamma(1-\lambda)(\omega^b)^2 + \lambda\alpha_b\textstyle\sum_{j\in N_i} W_j\varphi_{ij} + (1-\lambda)\beta^b\tfrac{1}{S^4}$$

Since $0 \leq W_j \leq 1$, $\sum_j W_j = 1$ and $\varphi_{ij} \in [0:1]$, the expression $\sum_{j\in N_i} W_j \simeq 1$; and the expression for a_1 can be reduced to,

$$a_1 = \gamma(1-\lambda)(\omega^b)^2 + \lambda\alpha_b + (1-\lambda)\beta^b \frac{1}{S^4}$$

The linear form equation in equation 4.29 corresponds to normal distribution for F_i^b. This makes sampling for F_i^b simple and fast:

$$F_i^b \sim N(F_0^b, \sigma_b)$$

where mean F_0^b and standard deviation σ_b are defined in the following way:

$$\frac{\partial U}{\partial F} = 0$$

$$2F_0^b a_1 - 2a_0 = 0, \tag{4.30}$$

which implies

$$F_0^b = \frac{a_0}{a_1} \tag{4.31}$$

Then the second partial derivative of the total energy is taken and equated with the second partial derivative of the normal distribution in order to get the standard deviation. i.e

$$\frac{\partial U(F_i|P_i, D_i)^2}{\partial {F_i^b}^2} = 2a_1 \tag{4.32}$$

and for a normal distribution

$$U(F_i|P_i, D_i) = \frac{(F^b - F_0^b)^2}{2\sigma_b^2} \tag{4.33}$$

which implies,

$$\frac{\partial U(F_i|P_i, D_i)^2}{\partial {F_i^b}^2} = \frac{1}{\sigma_b^2} \tag{4.34}$$

Equating equation 4.32 and 4.34 and considering the Gibbs sampler in simulated annealing,

$$\sigma_b = \sqrt{\frac{T}{2a_1}} \tag{4.35}$$

The modified simulated annealing algorithm that is adopted in this research performs as follows:

Begin

Determine the neighborhood system and parameters for the energy function

1. set the temperature, $T_k = T_0$
2. Initialize image configuration for the pan-sharpened image $F(i, j, b)$
3. For each pixel F_i^b generate $F'(i, j, b)$ for all bands using the Gibbs random sampler with mean equal to F_0^b and standard deviation σ_b as given in equation 4.31 and 4.35 respectively

$$F_i'^b \sim N(F_0^b, \sigma_b)$$

4. repeat steps (3) and (4) number of iteration times
5. Let $T_{k+1} = T_k \times \sigma$
6. Repeat steps (3)-(5) until T reaches 0 (gets frozen) or until three consecutive iterations give the same energies.

End

parameters used and to be estimated

The following parameters are used.

1. S which is the scale factor between the multispectral and the panchromatic image that is mainly important to determine the window size and generate the neighborhood system, a value $S = 4$ is chosen as the multispectral image is $4m$ resolution and the panchromatic image is $1m$ resolution
2. $\omega^b = 0.25$ for each band (assumed) that weights the contribution of each high spatial resolution multispectral band to the panchromatic image, the contribution of each band is assumed to be equal and their sum is equals 1 (as the panchromatic image is one band image).
3. $\alpha_b = 1$ for each band (assumed) which is the relevance of the different bands for the prior energy, the relevance of each band is assumed to be equal and there is no band that has a greater or lesser contribution for the prior energy.

The following parameters are to be experimentally estimated in the next chapter. (Optimal values depend on S, ω^b,α_b)

1. T_0 which is the initial temperature in the simulated annealing algorithm,

2. σ which is the temperature updating factor used to calculate the next temperature value,
3. λ which is the smoothness parameter that shows the contribution of the prior energy to the total energy,
4. W_{size} which is the window size that determines the neighborhood system useful in the determination of the prior energy,
5. β which is the inverse of the variance of the noise that was assumed to be Gaussian in relating the multispectarl image with the pan-sharpened image. It is assumed to be $(1, 1, 1, 1)$ for each band at first and to be estimated later experimentally.
6. γ which is the inverse of the variance of the noise that was assumed to be Gaussian in relating the panchromatic image with the pan-sharpened image. It is assumed to be 2 at first and to be estimated later experimentally.
7. ρ which is a parameter used to determine edges for the pan-sharpened image.

4.5 Accuracy assessment

Once the optimized pan-sharpened image has been obtained, it is common and necessary to evaluate accuracy against the reference image data. In this study accuracy can be understood as the level of agreement between grey values of the pan-sharpened image obtained using the method and the reference image.

4.5.1 Correlation coefficient

One of the quality measures that can be used to compare the level of agreement is the correlation or the correlation coefficient. This measure indicates the strength and direction of a linear relationship between two variables. In general statistical usage, correlation or co-relation refers to the departure of two variables from independence. There are different types of correlation coefficients. The best known is the Pearson-moment correlation coefficient. It is obtained by dividing the covariance, Cov, (measures how much the two variables vary together) of the two variables by their standard deviations [2]. In this study the two variables to be compared are the pan-sharpened image denoted by F and the reference image denoted by Ref.

The correlation $Corr_{(F,Ref)}$ between the two images F and Ref with expected values (the sum of the probability of each possible outcome of an experiment multiplied by the outcome value) μ_F and μ_{Ref} and standard deviations σ_F and σ_{Ref} is defined as:

$$Corr_{F,Ref} = \frac{E(FRef) - E(F)E(Ref)}{\sqrt{E(F^2) - E^2(F)}\sqrt{E((Ref)^2) - E^2(Ref)}} \tag{4.36}$$

Correlation is defined only if both the standard deviations are finite and both of them are nonzero. The correlation is 1 if there is an increasing linear relationship, -1 if there is a decreasing linear relationship, and some value in between in all other cases. As the correlation value gets closer to -1 or 1 the correlation between the variables will be stronger. If the variables are independent then the correlation is 0. A significant positive correlation exists between two variables if the correlation is from 0.5 to 1 [2].

4.5.2 Root mean square error

In statistics the root mean square error is used to describe accuracy including both random and systematic errors. The sum of the square of the differences between corresponding grey values of the reference image Ref and the pan-sharpened image divided by the total number of pixels gives the mean square error (MSE). The square root of this value is called the root mean square error (RMSE).

$$RMSE = \frac{1}{(M * N)} \sqrt{\sum (Ref - F)^2}, \tag{4.37}$$

where M and N are the number of rows and columns of the image respectively. The RMSE tells the average value at which the pixel value of the pan-sharpened image differs from the pixel values of the reference image. The highest value of the RMSE is dependent on the value of the data. It may be 0 or a positive value.

In this study the correlation and the RMSE between the pan-sharpened image and the reference image will be computed. These accuracy validation methods will also be used in experiments on estimating optimal values for the parameters. Besides they will also be used to compare the method developed with other pan-sharpening methods.

Chapter 5

Results and Discussions

This chapter illustrates the experimental results that are obtained in the process of MRF & SA - based image pan-sharpening including the analysis of the results. The first section, section 5.1, presents the experimental results done to check the performance of the method on synthetic data I. Section 5.2 describes the experimental results that are done in the determination of optimal values for the parameters that need to be estimated using the synthetic data II (degraded IKONOS image). Section 5.3 presents a result of the method using the optimal parameter values on the larger subsets of the QuickBird image. Section 5.4 presents the accuracy assessment and comparison of performance of the method with other existing pan-sharpening methods. Lastly section 5.5 winds up the chapter summarizing the findings of the results of the experiments.

5.1 Experimental results from the synthetic data I

Labeling at the first step was done randomly in the initial pan-sharpened image and therefore the image is distorted and has many isolated pixels and noisy appearance. In this experiment the main objective was to check the performance of the method using a visual comparison between the initial pan-sharpened image and the optimized pan-sharpened image, the curves of the total energy, and the RMSE. If these curves are decreasing smoothly as the number of iterations are increasing, it is considered as a good evidence for the method to work and proceed looking for optimal values using synthetic data II and use these optimal values on the remotely sensed images. For this purpose several experiments were done using the assumed parameters by changing the parameters that need to be estimated. The following parameters are used:

1. a scale factor S of 4, as the scale factor between the multispectral and the panchromatic image is 4.

2. $\omega^b = 0.25$ which is the assumed contribution of each high spatial resolution multispectral band to the panchromatic image, the contribution is assumed to be equal for each band and the sum equals 1.

3. $\alpha_b = 1$ which is the assumed relevance of the different bands for the prior

energy, each band is assumed to have equal contribution for the prior energy.

4. $\beta = (1, 1, 1, 1)$ which is the assumed inverse of the variance of the noise that was assumed to be Gaussian in relating the multispectarl image with the pan-sharpened image and,

5. $\gamma = 2$ which is the assumed inverse of the variance of the noise that was assumed to be Gaussian in relating the panchromatic image with the pan-sharpened image.

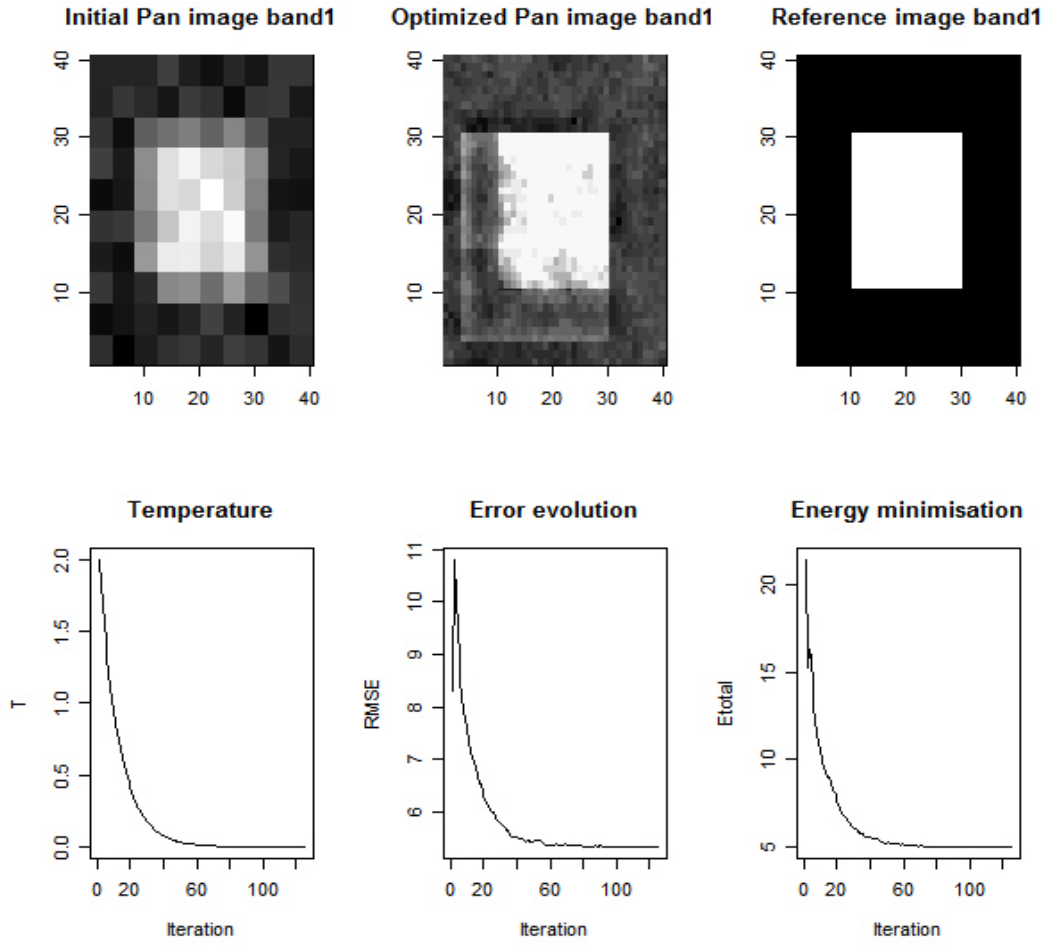

Figure 5.1: *Figure showing the initial (top left) and the optimized (top middle) pan-sharpened and the reference (top right) band & the temperature (bottom left), the RMSE (bottom middle) and the energy (bottom right) plots for synthetic image band1.*

In this experiment the last two parameters are assumed fixed. Several experiments were done to find optimal values for the initial temperature parameter T_0, for the temperature updating factor parameter σ, for the smoothness parameter λ, for the appropriate window size W_{size} and for the edge determiner

parameter ρ. An initial temperature value of 2, a temperature updating factor value between 0.5 and 0.9, a smoothness parameter of 0.1, a window size of 1 and a ρ value of 22^2 showed a good result for the synthetic image. Figure 5.1 shows a result at $T_0 = 2$, $\sigma = 0.5$, $\lambda = 0.1$, $W_{size} = 1$ and $\rho = 22^2$. The number of iterations required for SA to converge depends on the parameter values. The correlation and the RMSE between the optimized pan-sharpened image and the reference image were equal to 0.943 and 5.45 respectively. The total energy was equal to 5.13 and the optimization process stopped after 124 iterations. Figure 5.1 shows the initial and the optimized pan-sharpened and the reference bands & the temperature, the RMSE and the energy plots for synthetic image band 1. Note that these parameter values are not the "best optimal" values. But since the initial temperature parameter for synthetic data II is first estimated, the values of these parameters are used as the starting optimal values. Having done this synthetic data II are used (as they are synthesized from remotely sensed data) to estimate optimal parameter values.

5.2 Experimental results from synthetic data II

Estimating proper values of the parameters is the most important part of this research. In the following sub-sections proper values for the initial temperature parameter (T_0), for the temperature updating factor parameter (σ), for the smoothness parameter (λ), for the appropriate window size (W_{size}), for β and γ and for ρ parameters will be estimated. In each process the program is applied at least five times in order to get a consistent result and determined the mean and the standard deviation of the correlation and the RMSE values. These values are used to measure the quality of the pan-sharpened image and compare a result obtained using one parameter from a result using another parameter.

5.2.1 Effect of initial temperature T_0

One of the parameters that need to be determined is the initial temperature T_0. So the main objective of this experiment was to determine a proper value for it. To estimate this parameter the optimal values determined for synthetic data I are used. i.e. a σ factor of 0.5 , a λ value of 0.1, a W_{size} of 1 and a ρ value of 22^2. The experiments were done for values of T_0 between 0 and 10. For each T_0 value the method was applied 10 times from which the mean and the standard deviation values for the correlation, the RMSE and total energy were determined. The summary is as shown in tables A.1, A.2 and A.3 in appendix A. As it can be seen from the tables at T_0 values between 2 and 10 the optimized pan-sharpened image has a higher accuracy. As the value of T_0 increases almost a similar but less accuracy can be obtained. But the number of iterations needed for convergence is larger which makes the algorithm slower to reach to a freezing point and make computationally intensive.

The plots in figure 5.2 show the correlation and the RMSE of the optimized pan-sharpened image with the reference image and the total energy of the optimized pan-sharpened image. They also reveal that for T_0 = 5, 7 and 10 there is a large

deviation between the minimum and the maximum values. Relatively, highest correlation, lowest mean square error and lowest total energy is obtained at $T_0 = 2$.

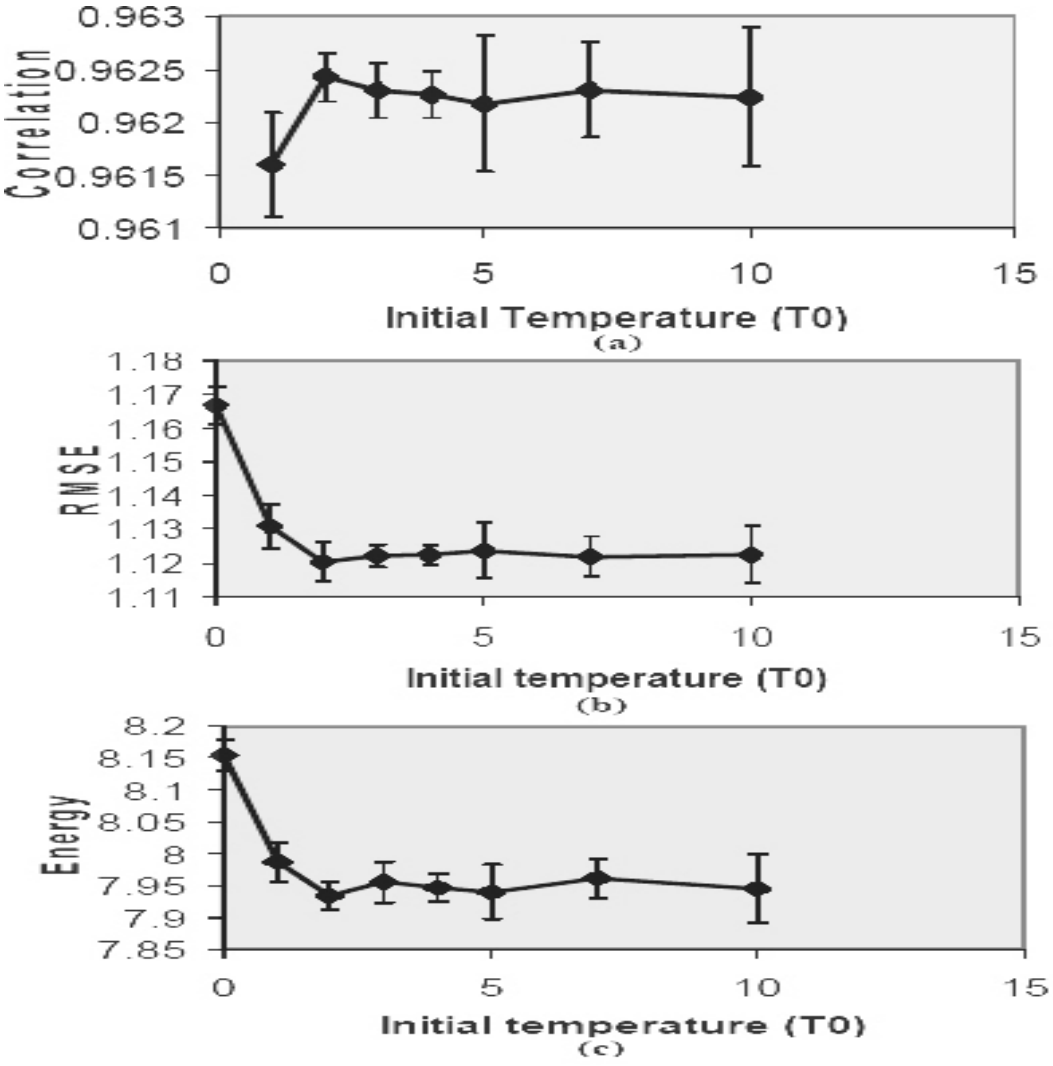

Figure 5.2: *Figure showing the plots for the correlation (a), RMSE (b), and total energy (c) of the optimized pan-sharpened for searching optimal T_0 value (Energy value is normalized by the number of pixels and error bars represent standard deviation of the values).*

Since the variation in the accuracy is very small a T_0 value of 3 or 4 can also be used. The experimental finding was in line with other previous works on MRF. For instance in the books by Tso & Mather and Li [26, 24] it is stated that an initial temperature value between 2 and 4 can result in a good result. Recent works by Kasetkasem and Rahel [21, 33] on MRF also worked well at $T_0 = 2$ and 3.

5.2.2 Effect of temperature updating factor σ

Using the optimal value found in the above experiment, T_0=2, and keeping the other parameters constant, this experiment was aimed at looking for an optimal value for the temperature updating factor σ at which optimum pan-sharpened image can be obtained. The experiments were done varying the σ value from 0.1 to 0.9 and from 0.91 to 0.99. For each σ value the program was applied 10 times from which the mean, and the standard deviation values for the correlation, the RMSE and total energy are determined.

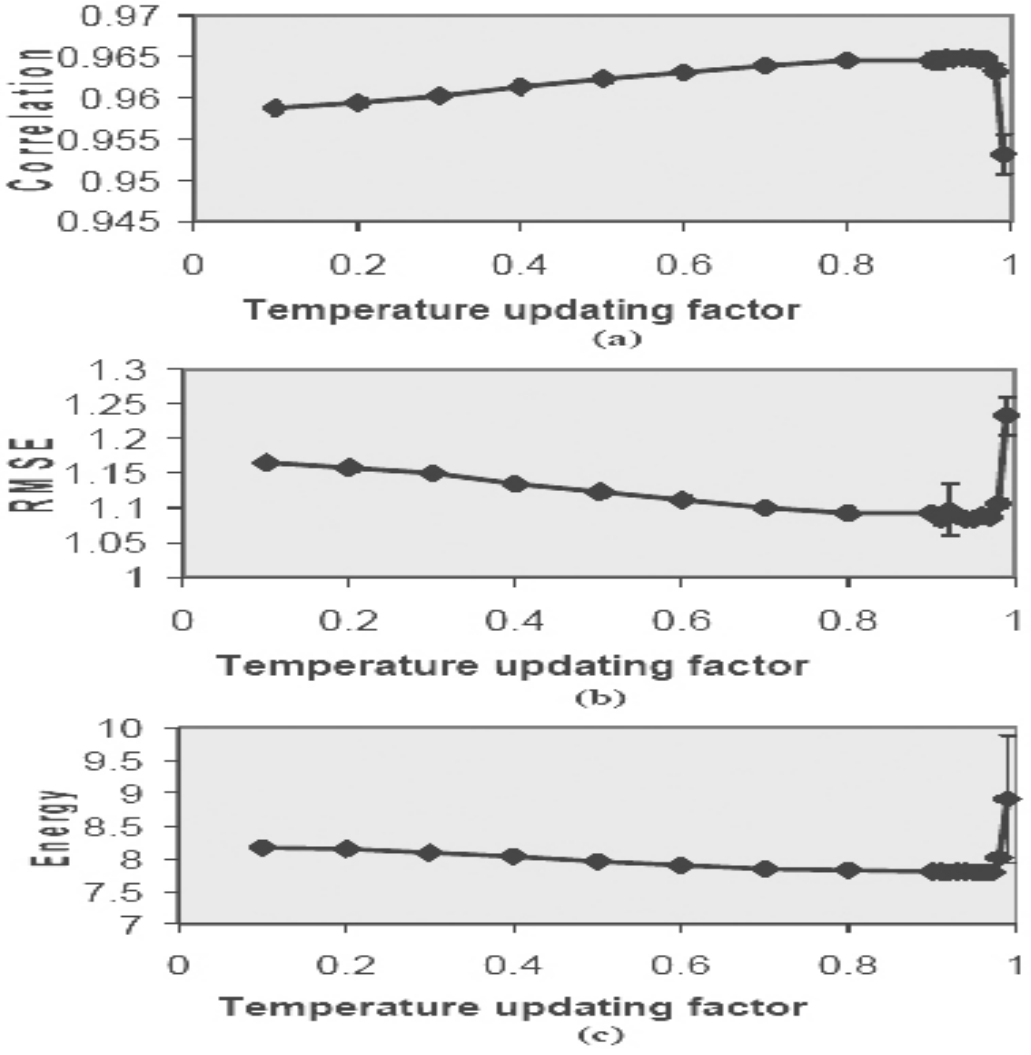

Figure 5.3: *Figure showing the plots for the correlation (a), RMSE (b), and total energy (c) of the optimized pan-sharpened for searching optimal σ value (Energy value is normalized by the number of pixels and error bars represent standard deviation of the values).*

The summary is as shown in tables B.1, B.2 and B.3 in appendix B. As it can be seen from the tables at $\sigma = 0.8$ and 0.9 the optimized pan-sharpened image has a higher accuracy. Further a best optimal value for σ was looked for between

0.9 and 0.99. The experiments reveal that at σ = 0.92 relatively a best optimal value can be found. In fact for values between 0.9 and 0.97 the results are almost similar. The plots in figure 5.3 show the correlation and the RMSE of the optimized pan-sharpened image with the reference image and the total energy of the optimized pan-sharpened image. They show that there is a high correlation, low mean square error and low total energy for a σ value between 0.8 and 0.97. The results from the tables and the plots show that one can set the value of this parameter at 0.92 in order to get a best optimal pan-sharpened image.

5.2.3 Effect of smoothness parameter λ

The smoothness parameter λ that is used to make a balance between the con-

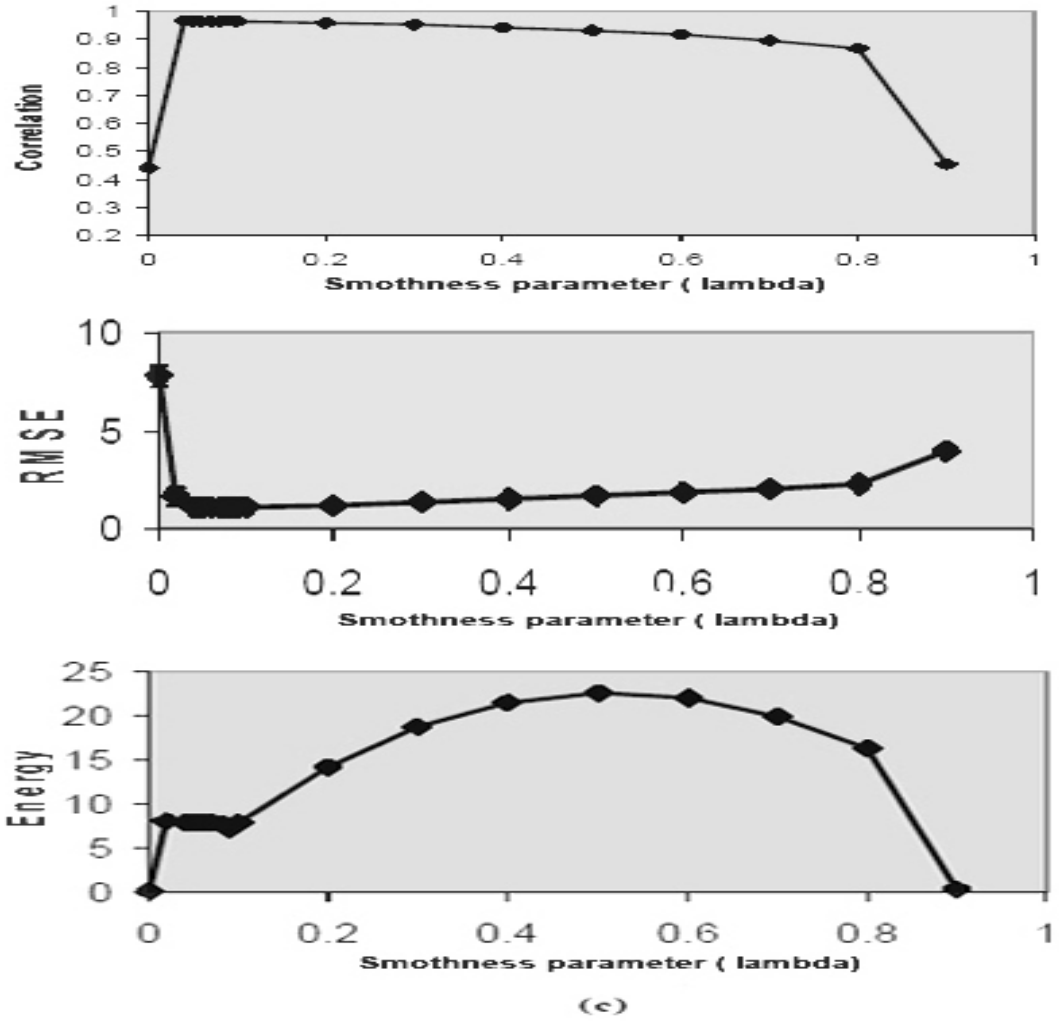

Figure 5.4: *Figure showing the plots for the correlation (a), RMSE (b), and total energy (c) of the optimized pan-sharpened for searching optimal λ value (Energy value is normalized by the number of pixels and error bars represent standard deviation of the values).*

ditional energies and the prior energy in the optimization process is an other parameter that has to be optimized. This parameter determines the smoothness of the pan-sharpened image. The experiment was done using the above optimal values obtained (i.e $T_0 = 2$ and $\sigma = 0.92$) and keeping the other parameters constant. The experiments were done changing the value of λ from 0 to 0.9. For each λ value each experiment was repeated ten times and the mean, and the standard deviation values for the correlation, the RMSE and total energy were calculated.

Tables C.1, C.2 and C.3 in appendix C show the summary of the results. From the experiments it is found that for λ values of 0.1 and 0.2 the accuracies are higher than other values. After this result is found further experiments were made for λ values between 0 and 0.09 in order to set a relatively best value for it. The result shows that highest accuracy can be found at λ = 0.09. The plots in figure 5.4 show the correlation and the RMSE of the optimized pan-sharpened image with the reference image and the total energy of the optimized pan-sharpened image. Both the table and the plots reveal that one can set the value of λ between 0.08 and 0.2. In fact the accuracy at $\lambda = 0.09$ is the best. The result indicates that the contribution of smoothness for the pan-sharpened image is small. But making this value smaller (near to 0) makes the result worse and making the value greater than 0.8 brings a worst result even if the total energy seem to decrease to zero.

5.2.4 Effect of neighborhood size W_{size}

The window size is one of the parameters that need to be determined experimentally. A larger window size allows a value for a pixel to be determined based on more neighborhood pixels. The window size determines the effect of smoothness of the image and hence the contribution of the prior energy for the total energy. The experiments were done using the optimal values obtained in the above sections ($T_0 = 2, \sigma = 0.92$ and $\lambda = 0.09$). A window size of 1, 3, 5 and 7 were chosen for the experiments. For each value of W_{size} the experiment was repeated ten times and the mean, and the standard deviation values for the correlation, the RMSE and total energy were calculated.

Table D.1 in appendix D gives the summary of the results. The results revealed that higher accuracy (higher correlation, lower RMSE and lower total energy) was found for a window size of 1. This means a contextual information collected from neighborhood pixels of window size 1 was enough in the determination of the prior information. The plots in figure 5.5 show the correlation and the RMSE of the optimized pan-sharpened image with the reference image and the total energy of the optimized pan-sharpened image. The results from the plots also show that a window size of 1 was enough to get an optimal pan-sharpened image.

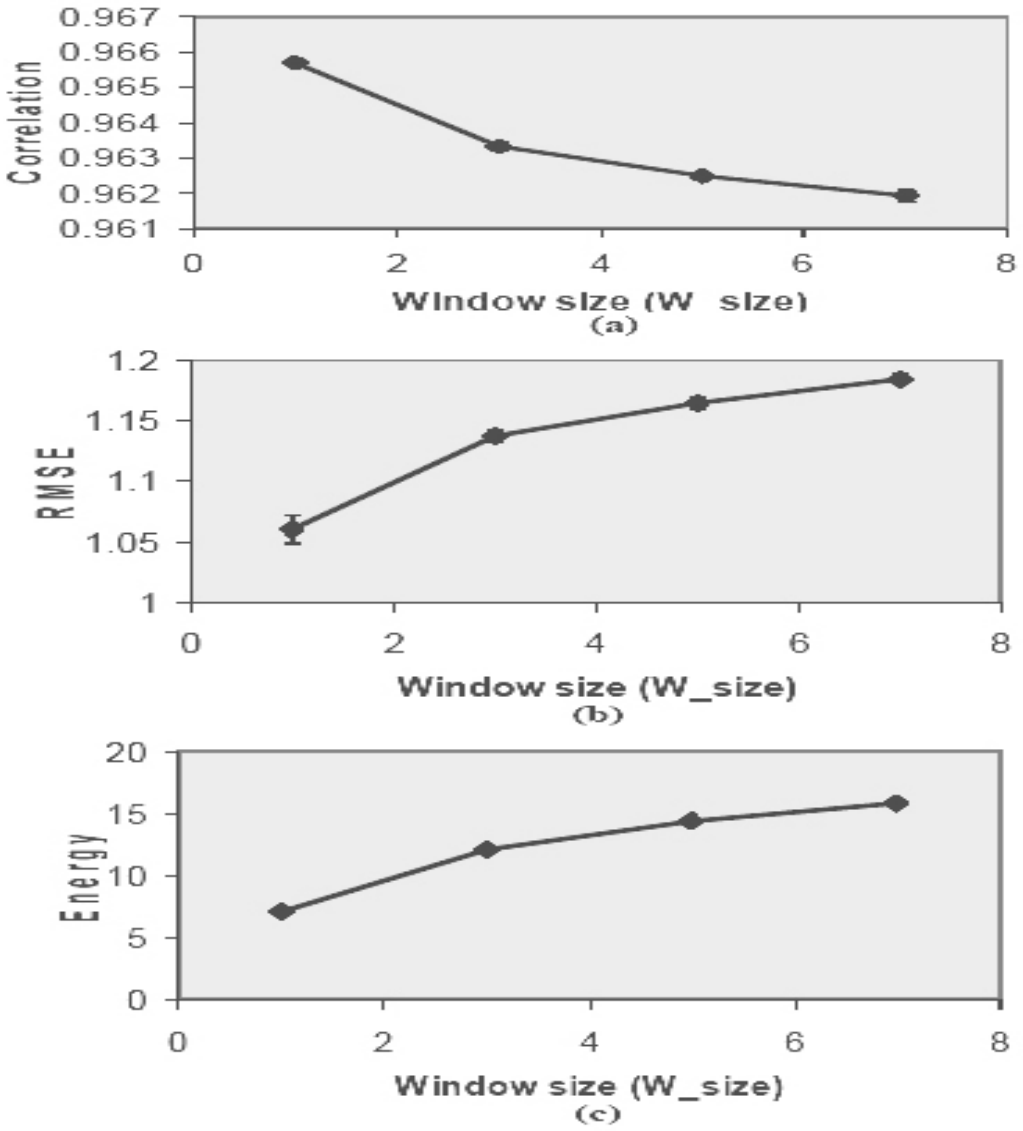

Figure 5.5: *Figure showing the plots for the correlation (a), RMSE (b), and total energy (c) of the optimized pan-sharpened for searching optimal W_{size} value (Energy value is normalized by the number of pixels and error bars represent standard deviation of the values).*

5.2.5 Effect of parameters β & γ

In this experiment optimal values are determined for the parameters β and γ. These parameters control the contributions from the two likelihood models (multispectral and panchromatic). β and γ were assumed to be 1 and 2 in looking for optimal values for the other parameters in the above sections. The experiments were done changing the values of the two parameters proportionally (when $\gamma = 0$ $\beta = 1$, when $\gamma = 0.25$ $\beta = 4$, when $\gamma = 0.5$ $\beta = 2$ etc.) from 0 to 16 for γ and from 1 to 0.0625 for β using the optimal values of $T_0 = 2$, $\sigma = 0.92$,

$\lambda = 0.09$ and $W_{size} = 1$ obtained from the above experiments. Each experiment

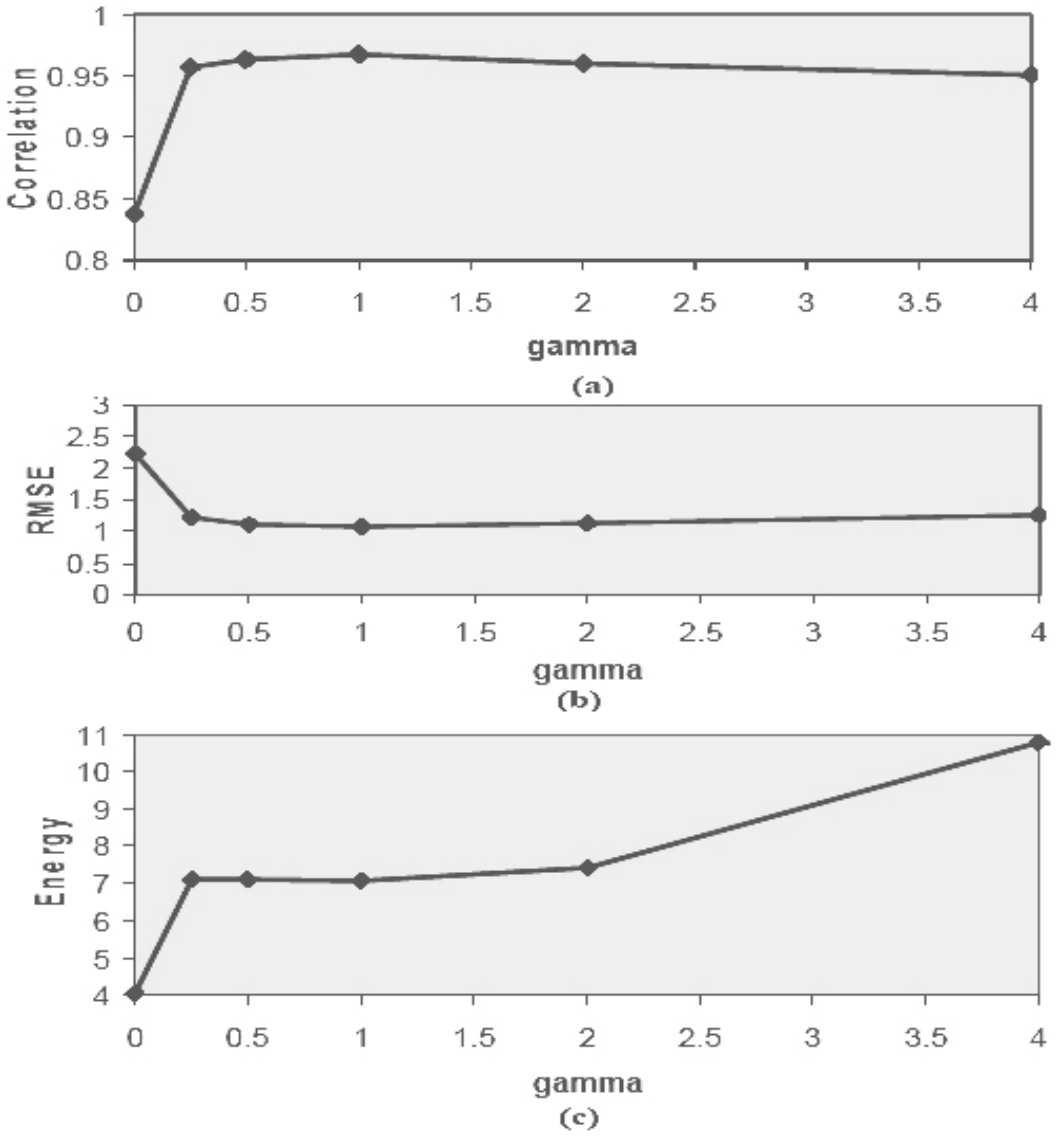

Figure 5.6: *Figure showing the plots for the correlation (a), RMSE (b), and total energy (c) of the optimized pan-sharpened for searching optimal β & γ values (Energy value is normalized by the number of pixels and error bars represent standard deviation of the values).*

was repeated 5 times from which means of correlation, RMSE and total energy are calculated.

Table 5.1 shows the summary of the results. The plots in figure 5.6 show the correlation and the RMSE of the optimized pan-sharpened image with the reference image and the total energy of the optimized pan-sharpened image. The plots show the correlation, the RMSE and the total energy when the value of γ is changing. But since the two parameters are changed proportionally in the

Table 5.1: *Summary of the result in searching optimal β & γ value*

γ	β	*Mean Corr*	*Mean RMSE*	*Mean Total Energy*
0	1	0.837	2.24	4.05
0.25	4	0.957	1.22	7.08
0.5	2	0.964	1.12	7.10
1	1	0.967	1.07	7.07
2	0.5	0.961	1.13	7.43
4	0.25	0.950	1.26	10.79
16	0.0625	0.867	2.21	7.98

experiment the pattern of the plot also holds true for the parameter β. Both the plots and the table show that optimal pan-sharpened image can be obtained when $\beta = \gamma = 1$.

5.2.6 Effect of parameter ρ

The parameter ρ is one of the parameters that need to be determined experimentally. This parameter is used to determine edges in the pan-sharpened image. The experiments were done using the optimal values obtained in the above sections ($T_0 = 2, \sigma = 0.92$ and $\lambda = 0.09$, and $\beta = \gamma = W_{size} = 1$). Experiments were done for ρ value of $10^2, 15^2, 20^2, 21^2, 22^2, 23^2, 25^2$ and 30^2.

Table 5.2: *Summary of the result in searching optimal ρ value*

ρ	*Mean Corr*	*Mean RMSE*	*Mean Total Energy*
10^2	0.937	3.11	10.02
15^2	0.945	2.82	9.06
20^2	0.955	2.56	8.42
21^2	0.957	2.32	8.01
22^2	0.967	1.07	7.07
23^2	0.952	2.34	8.50
25^2	0.948	2.54	8.62
30^2	0.941	2.73	8.87

Table 5.2 shows the summary of the results. The plots in figure 5.7 show the correlation and the RMSE of the optimized pan-sharpened image with the reference image and the total energy of the optimized pan-sharpened image. Both the table and the plots show that optimal solution was obtained at $\rho = 22^2$.

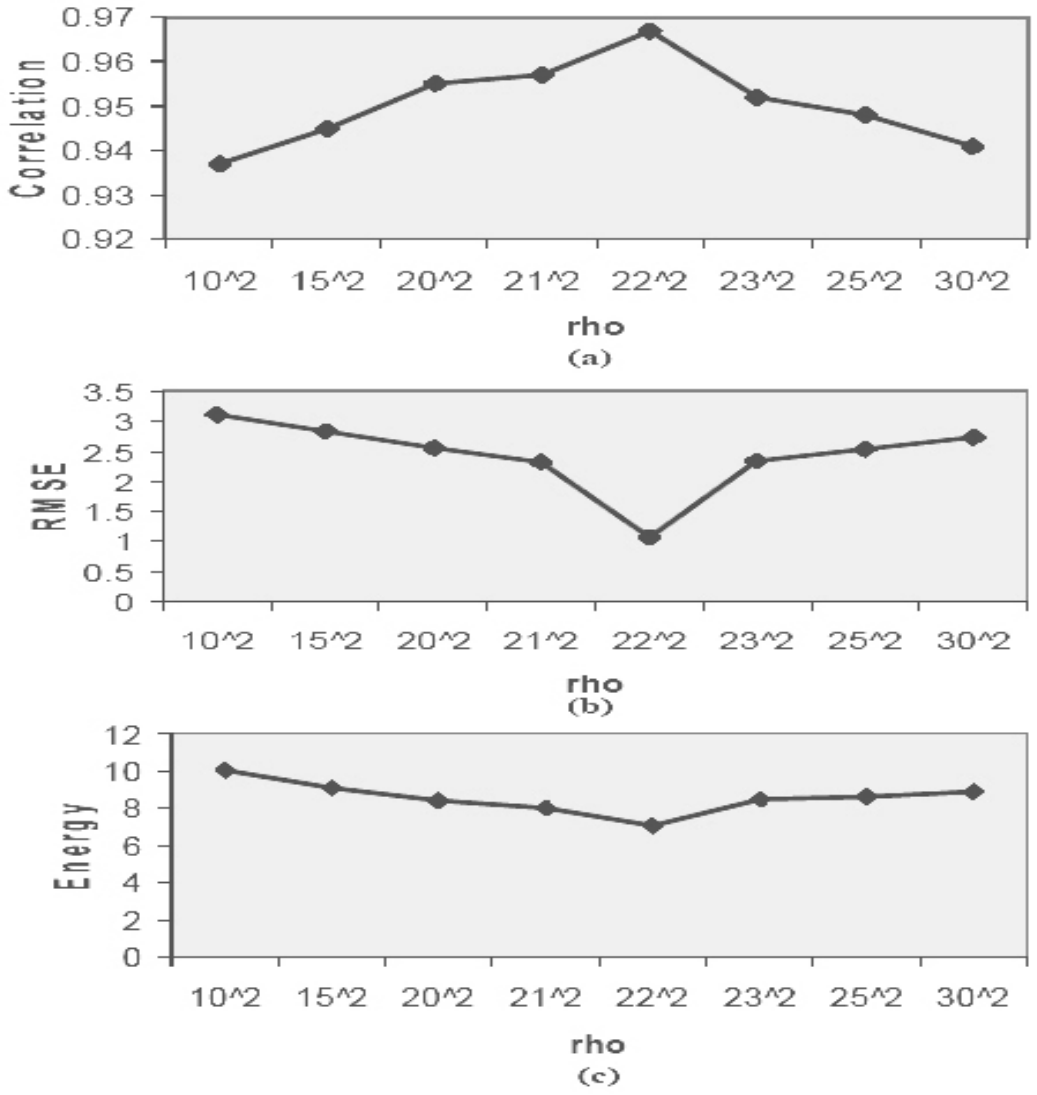

Figure 5.7: *Figure showing the plots for the correlation (a), RMSE (b), and total energy (c) of the optimized pan-sharpened for searching optimal ρ value using optimal values from synthetic data II (Energy value is normalized by the number of pixels and error bars represent standard deviation of the values).*

5.2.7 Control experiment for the initial temperature T_0

As explained in section 5.2.1, initially optimal value for the initial temperature was found using the other optimal values obtained from synthetic data I. In this control experiment optimal value for it was determined, this time with the optimal values obtained from the experiments in sections 5.2.2 to 5.2.5 (i.e. $\sigma = 0.92$, $\lambda = 0.09$, $W_{size} = \beta = \gamma = 1$ and $rho = 22^2$. The experiment was done for the value of T_0 between 0 and 10. For each T_0 value the method was applied 5 times from which the mean and the standard deviation values for the

correlation, RMSE and total energy were determined.

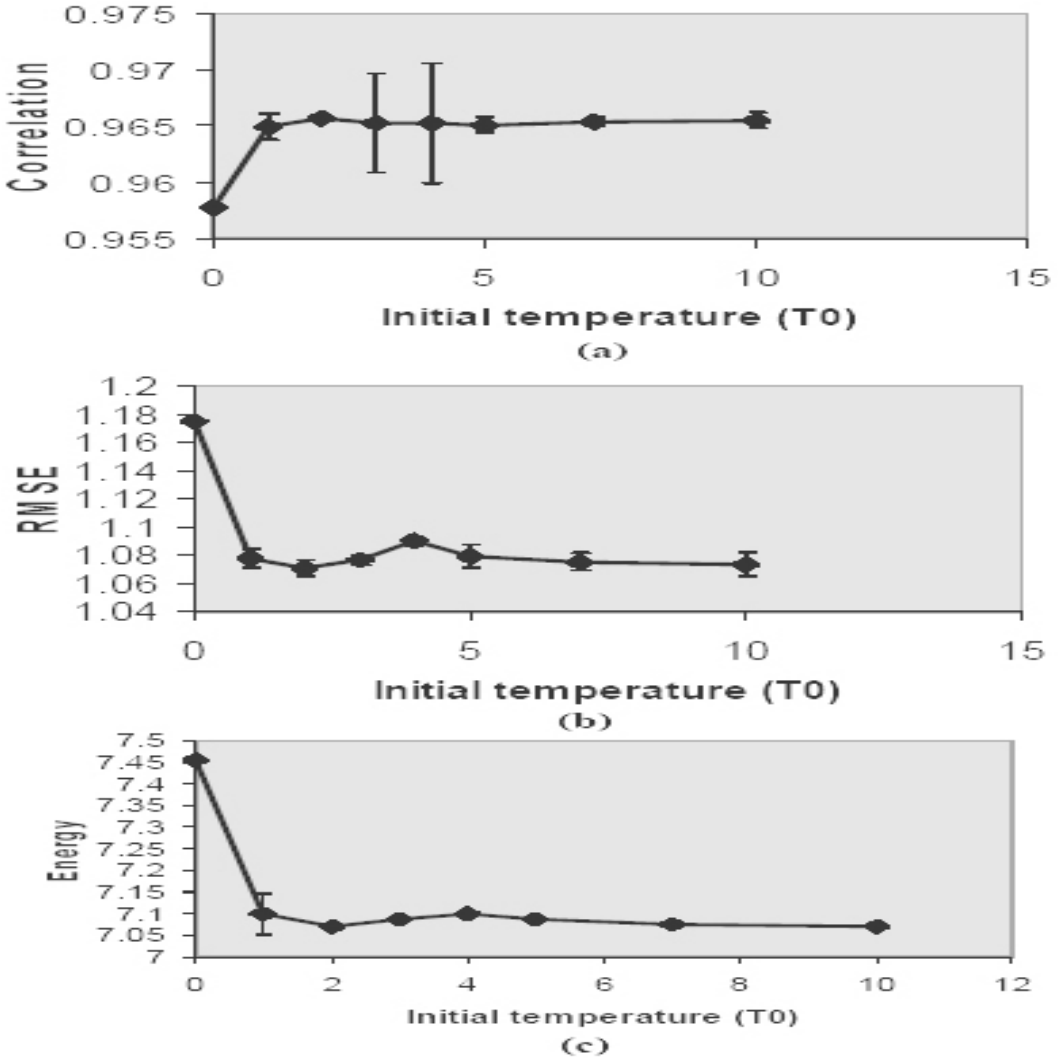

Figure 5.8: *Figure showing the plots for the correlation (a), RMSE (b), and total energy (c) of the optimized pan-sharpened for searching optimal T_0 value using optimal values from synthetic data II (Energy value is normalized by the number of pixels and error bars represent standard deviation of the values).*

Tables E.1, E.2 and E.3 in appendix E show the summary of the result. Similar to the result of the experiments obtained using the optimal values from synthetic data I, at T_0 = 2, 3, 4, 5, 7 and 10 the optimized pan-sharpened image has a higher accuracy. As the value of T_0 increases almost a similar but less accuracy can be obtained. But the number of iterations needed to finish processing is larger which makes the algorithm slower to reach to a freezing point and make computationally intensive. Figure 5.8 show the plots for the correlation and RMSE of the optimized pan-sharpened image with the reference image and the total energy of the optimized pan-sharpened image. They show that rela-

tively highest correlation, lowest mean square error and lowest total energy is obtained at T_0 = 2. Since the variation in the accuracy is very small an initial temperature T_0 value of 3 or 4 can also be used. Again like that of the experimental results in section 5.2.1 the experimental finding was in line with other previous works on MRF showing that an initial temperature value between 2 and 4 can give a good result.

5.3 Pan-sharpening from the QuickBird image

In the above sections appropriate optimal values are determined experimentally for the parameters to be estimated. Here using the method illustration will be given on the QuickBird image described in section 3.2.1.

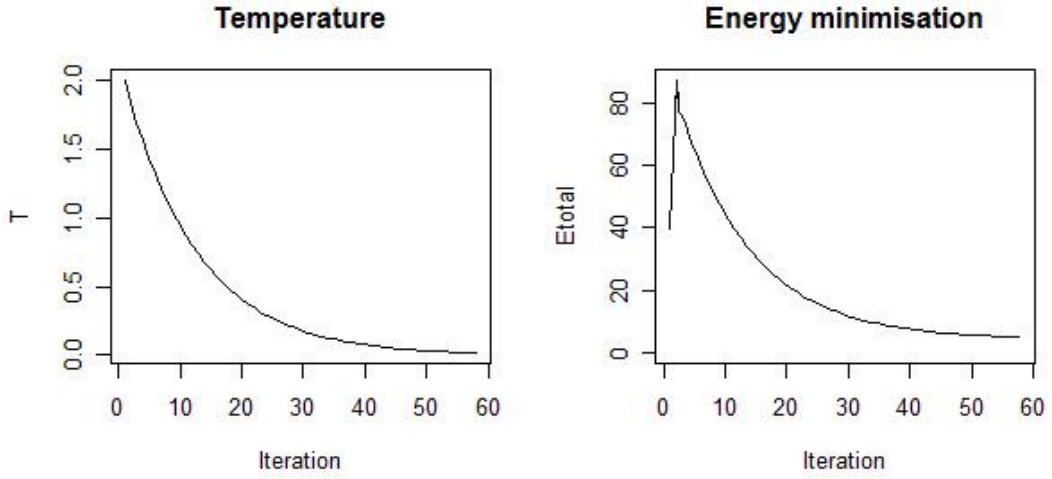

Figure 5.9: *Figure showing the plots for the temperature and the total energy curves*

The optimal values for the initial temperature T_0, for the temperature updating factor σ, for the smoothness parameter λ, for the window size W_{size}, for γ, for β and ρ are found to be 2, 0.92, 0.09, 1, 1, 1, and 22^2 respectively. Since QuickBird image has similar characteristics as the IKONOS image, the same parameter values are used and the method is applied on relatively larger subsets (120×120 panchromatic and a corresponding 30×30 multispectral) of the QuickBird images.

Figure 5.9 shows the curves for the temperature parameter and for the total energy. Both curves are decreasing as the number of iteration is increased. The process converged after 59 iterations. Figure 5.10 shows the input panchromatic and multispectral images. Figure 5.11 shows the pan-sharpened image obtained from the two images. As it can be seen from the result in the pan-sharpened image the spatial resolution of the multispectral image is increased via the panchromatic image keeping the spectral information from of the multispectral image. Since a reference image for this data set is not available qual-

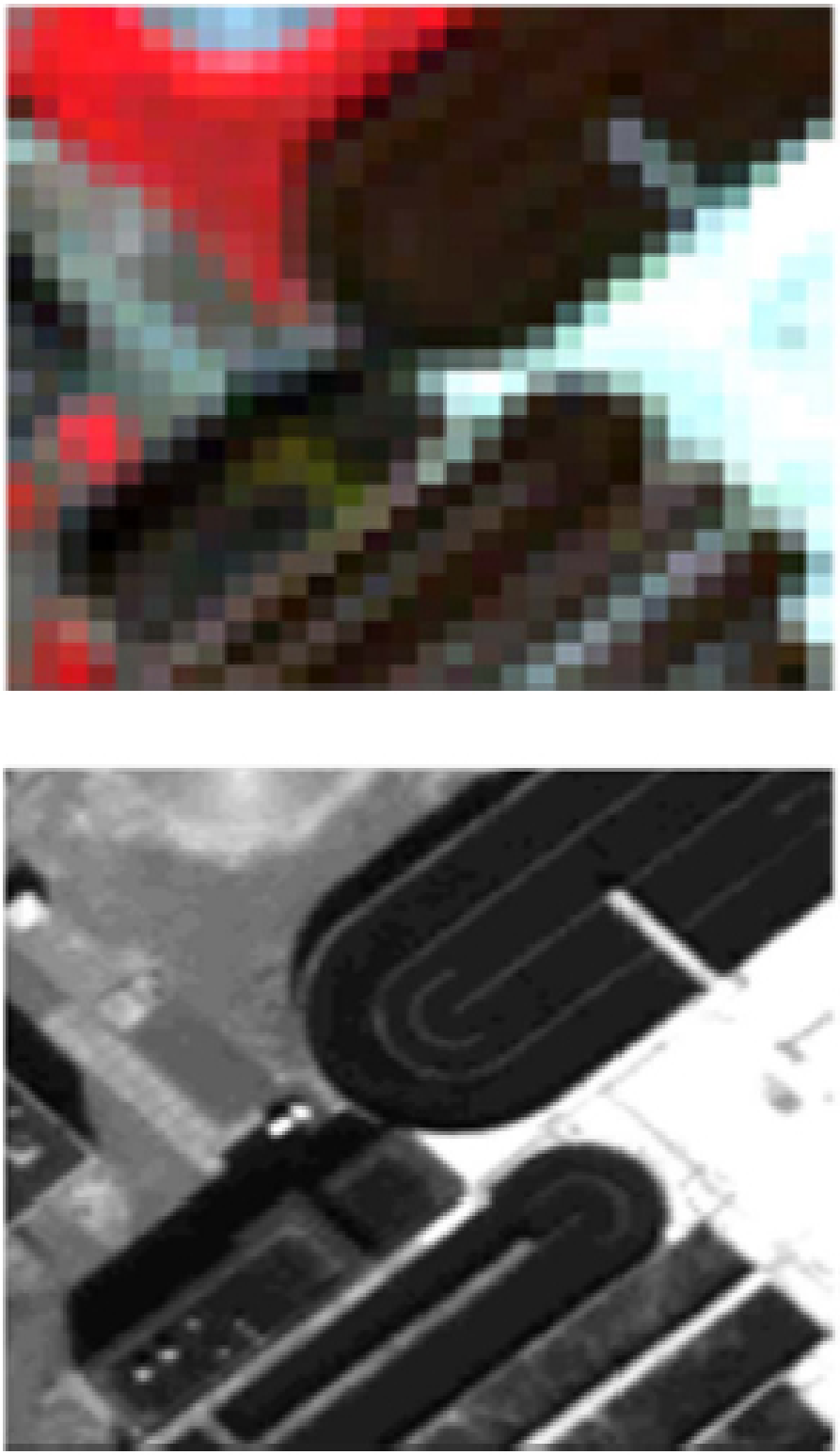

Figure 5.10: *Figure showing the multispectral image (top), the panchromatic image (bottom) for the QuickBird imagery*

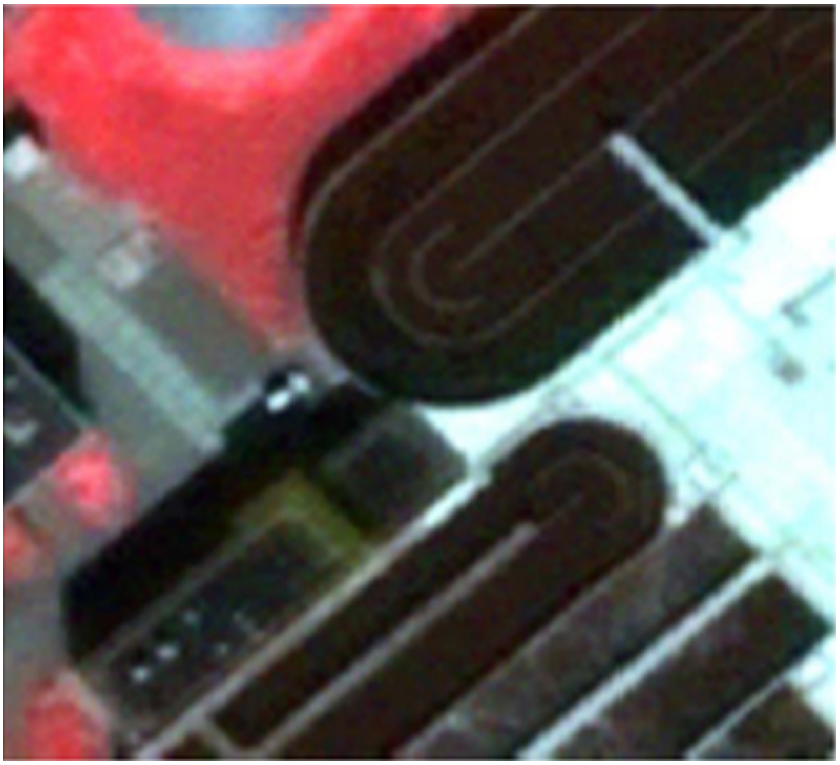

Figure 5.11: *Figure showing the pan-sharpened image for the QuickBird imagery*

itative assessment was done by visual comparison with the aerial photograph. Figure 5.12 shows the aerial photograph and the pan-sharpened image using natural color (3, 2, 1 band combination) side by side. The aerial photo is not in

Figure 5.12: *Figure showing the subset of an aerial photograph (left) and pan-sharpened image of the corresponding subset(right) of the QuickBird imagery*

fact exactly the same to that of the pan-sharpened image. The pan-sharpened

image has a better resolution that came from the panchromatic image. The aerial photograph is not also taken at the same time to that of the satellite images and the spectral information of the aerial photograph is not good. The quality of this pan-sharpened image can better be determined based on the result of the quality assessment for synthetic data II.

5.4 Accuracy assessment and performance comparison with other pan-sharpening methods

In this research accuracy assessment is done using the correlation coefficient and the RMSE between a reference image and a pan-sharpened image. The data set used for comparison is the synthetic data set II. Using the correlation coefficient and the RMSE a comparison is done between well known existing methods of image-pan-sharpening and the method developed in this research. Three wavelet methods (that use - a single band spectral transform, the IHS spectral transform and the principal component spectral transform - all implemented in ERDAS package), the Gram-Schmidt spectral sharpening method that is based on the component substitution strategy invented by Laben and Brover in 1998 and patented by Eastman Kodak, being implemented in the ENVI package [5],

Table 5.3: *Correlation coefficient and RMSE for the different methods of pan-sharpening using synthetic data II*

Pan-sharpening method	*Correlation*	*RMSE*
Wavelet (PC)	0.89	10.82
Wavelet (IHS)	0.91	10.44
Wavelet (single band)	0.92	9.45
Gram-Schmidt	0.91	9.56
MRF-ICM	0.95	1.18
MRF-SA	**0.97**	**1.07**

and the MRF-ICM pan-sharpening method (a method similar to the method developed by Molina et al. but extended to include edge preservation) are compared with the MRF-SA method of pan-sharpening.

Table 5.3 shows the correlation and the RMSE of the different existing methods of pan-sharpening and the new MRF-SA method developed in this study. The table reveals that the correlation for the MRF-SA method is the highest (0.97) as compared to the other methods. The RMSE for the MRF-SA method is also very small (1.07) as compared to the RMSE of the other methods. The accuracy of the MRF-ICM method is also higher but lesser than the MRF-SA method. But the processing time it takes is a bit lesser than the MRF-SA method. The other methods are also faster than the MRF-SA method. For the MRF-SA method the correlation and the RMSE was found to be (0.99, 1.33), (0.98, 1.49),

(0.96, 1.64) and (0.94, 3.46) for band 1 to 4 respectively in pairs. The result shows that the method performs nicely particularly for the first three bands. For these bands the correlation is very high and there is a very small error between pixel values of the reference image and the out image.

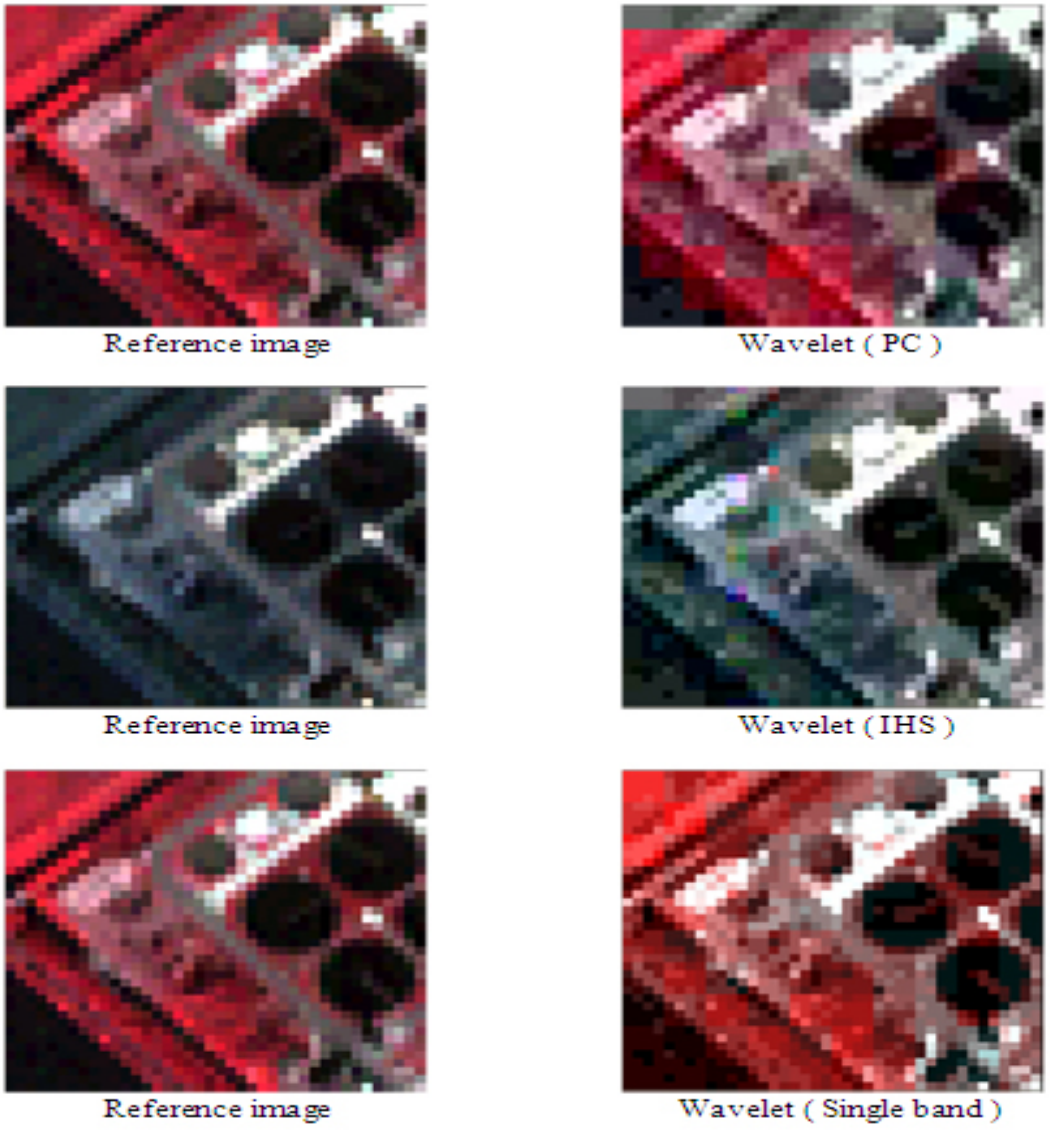

Figure 5.13: *Figure showing the reference image and pan-sharpened images obtained using the Wavelet methods*

The variation of accuracies for the different bands is because the spectral characteristics of the deferent bands is not studied very well in this study. Figure 5.13 shows the reference and the output images of the three Wavelet methods (the Wavelet PC method, the wavelet IHS method and the Wavelet single band method) of pan-sharpening. Figure 5.14 shows the reference and the output images for the other two methods including MRF-SA (the Gram-Schmidt method,

the MRF-ICM method and the MRF-SA method). Except for the Wavelet IHS method where the band combination is 3, 2, 1, the images are displayed in 4, 3, 2 band combination both in the reference and in the output images.

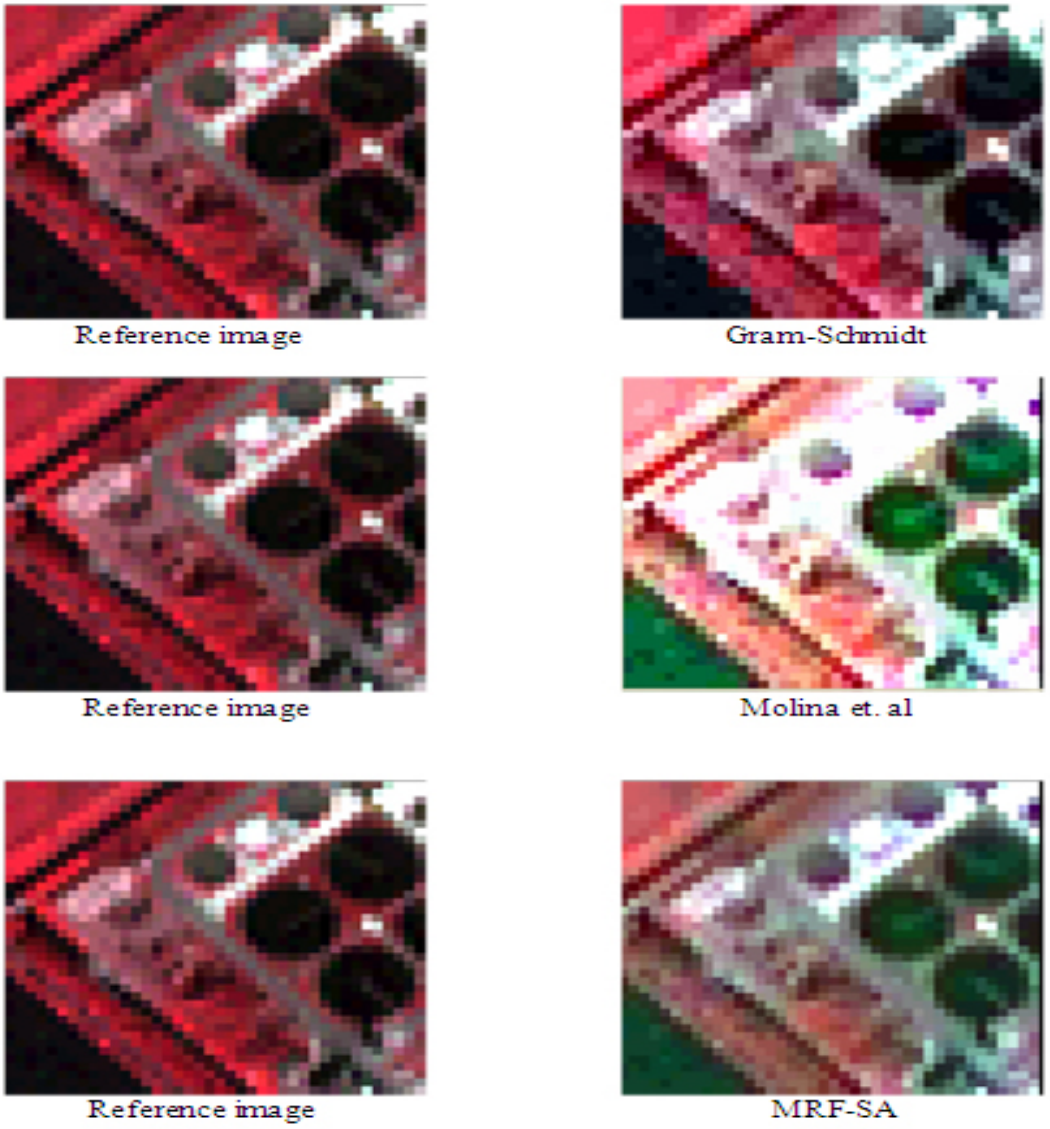

Figure 5.14: *Figure showing the reference image and pan-sharpened images obtained using the Gram-Schmidt, the MRF-ICM and the MRF-SA methods*

5.5 Summary of findings from results

The result of using the new method developed in this research on the synthetic imagery has proved the capability of the method for image pan-sharpening. The synthetic images show that the MRF-SA method produces a better pan-sharpened image than the known existing methods. The QuickBird image used

proved the method's performance on satellite images. The accuracy of the result rely on the scale factor, on the assumed parameters and on the optimal parameters that have an impact on the optimization process. The results from both the synthetic and the remotely sensed data proved the reliability of this new method for satellite image pan-sharpening.

Chapter 6

Conclusion and recommendations

6.1 Conclusion

The main objective of this study is to develop a new Bayesian method for image pan-sharpening using the Markov random field and the simulated annealing algorithm for satellite images that gives a *MAP* estimate for the pan-sharpened image. It has the following sub-objectives:

1. To formulate pan-sharpening as an image restoration model and to determine the parameters of this model by building observation and prior models.
2. To integrate the modeled prior information with the conditional information obtained from the multispectral and the panchromatic images using the Bayesian estimation in order to get the final pan-sharpened image and to find the optimal solution using the simulated annealing algorithm.
3. To assess the quality of the pan-sharpened image and,
4. To compare the new method with the already existing methods of pan-sharpening.

In order to address the objectives four corresponding questions were posed during this study. Experiments were done using synthetic and remote sensing data sets in order to answer the research questions. In chapter 5 the results obtained from the experiments were presented and discussed. This chapter gives a conclusion for the research from the perspective of the research objectives and questions. The performance of the new developed method is also discussed and few recommendations are given below for further research.

6.1.1 Model formulation, optimal parameter determination and optimization

One of the objectives of this research is to formulate image pan-sharpening as an image restoration model and to determine the parameters of this model by

modeling two models - prior and conditional models. One prior energy model using the MRF and two conditional energy models are developed. The three models are considered under the Bayesian framework and optimized using the simulated annealing algorithm to meet the second objective of this study.

Optimizing parameter values of the developed models is the other objective of the research. There are seven parameters for which optimal values were found experimentally. The first parameter is the initial temperature (T_0) used in the simulated annealing algorithm. This study revealed that an T_0 of 2 is works effectively. In addition an initial temperature T_0 value of 3 or 4 can also produce good results. The influence on the pan-sharpened image is very small for $T_0 = 2$ to 4.

The second parameter that determines the optimization process is the temperature updating factor σ, which refers to the decrease of the temperature parameter according to the designed schedule. Annealing is scheduled in a slow decreasing rate. This is because as T_0 decreases, samples from the posterior probability are forced towards the minimal energy configurations and this leads to a tight coupling between the neighboring pixels. The experimental results show that the optimal σ value found is 0.92. σ values between 0.9 and 0.97 can also give good results but larger values result into longer processing time.

The third parameter that influences the quality of a pan-sharpened image from MRF-SA method is the smoothing parameter λ. If the value of this parameter is larger than the optimal value there could be an over smoothing effect as the spectral information is ignored and if it is set below the optimal value there could be a noisy appearance due to the low weight given to the neighboring pixel information. An optimal value for $\lambda = 0.09$ was determined. Values between 0.08 and 0.2 can also give good results.

The fourth parameter that an optimal value was looked for was the window size (W_{size}). It determines the effect of smoothness of the image and hence the contribution of the prior energy for the total energy. A larger window size allows a value for a pixel to be determined based on more neighborhood pixels. On the contrary a smaller window size allows a value to be assigned for a pixel based on small number of neighborhood pixels. The experimental results revealed that a window size of 1 was a better estimate to get an optimally pan-sharpened image.

The fifth and sixth parameters for which optimal values were found to them experimentally were β and γ. Optimal value of 1 for both β and γ were found to give better results. This shows that equal contribution of conditional energies from the multispectral and panchromatic image can be taken to arrive at optimal solution.

The last parameter that an optimal value was determined is the parameter ρ

that is used to determine edges for the pan-sharpened image. Optimal value of 22^2 was found to give better result. In this study the design of the Gibbs sampler was found to be a novelty for the edge preserving energy.

6.1.2 The performance of the method and comparison with other methods

In this study a new method for image pan-sharpening is developed. The quality of the pan-sharpened image was assessed mainly using the correlation coefficient and the RMSE values. Results from the synthetic data II reveal that there is a very high correlation (0.97) and a very small RMSE (1.07) between the reference and the pan-sharpened image pixel values. Results from the satellite imagery also show that the method works effectively and most urban objects can be recognized because of color differences in the pan-sharpened image unlike that of the panchromatic image. Experimentation was also done to compare the method with five other existing well known pan-sharpening methods. The result shows that the MRF-SA method for image pan-sharpening performs better than the other methods at a cost of more computational time.

6.2 Recommendations

A new and reliable MRF-SA based pan-sharpening method for satellite images is developed in this research. Undoubtedly there exist some limitations that need to be solved in further researches. The following are some of the recommendations for future work:

1. It is recommended to take different image subsets and study the influence of image characteristics on the developed method.
2. It is also recommended to analyze image quality descriptors for the application of pan-sharpening and perform image quality analysis for the developed method.
3. Since the simulated annealing algorithm is time consuming due to its cooling schedule, it is recommended to implement the method in faster software than the R programming language and statistical computation software.

Bibliography

[1] Fundamental of remote sensing. Accessed on September , 2006, http://ccrs.nrcan.gc.ca.

[2] Wikipedia,the free encyclopedia. Accessed on January, 2007, http://en.wikipedia.org/wiki.

[3] programming in R. Accessed on september, 2006, http://faculty.ucr.edu/ tgirke/Documents/R_BioCond/R_Programming.html.

[4] Digitalglobe. Accessed on October, 2006, http://www.digitalglobe.com/about/quickbird.html.

[5] Ms + pan image fusion by an enhanced gram-schmidt spectral sharpening. Accessed on February, 2007, http://www.igik.edu.pl/earsel2006/abstracts/data_fusion/aiazzi_baronti.pdf.

[6] Satellit imaging corporation. Accessed on October, 2006, http://www.satimagingcorp.com/gallery-ikonos.html.

[7] L. Alparone A. Garzelli, B. Aiazzi and S. Baronti. An mtfbased spectral distortion minimizing model for pansharpening of very high resolution multispectral images of urban areas. In The 2nd GRSS/ISPRS Joint Workshop, editor, *Data fusion and remote sensing over urban areas*, page 9094, Berlin, 2003.

[8] Gurret C. Huurneman et al. *Principles of Remote sensing , An Introductory Text book*. Enschede , The Netherlands, ITC, 3 edition, 2004.

[9] Molina R. and Katsaggelos A.K Alvarez, L.D. High resolution images from a sequence of low resolution observations. *Digital Image Sequence Processing*, Compression and Analysis(9):233–259, 2004.

[10] Marc Berthod, Zoltan Kato, Shan Yu, and Josiane Zerubia. Bayesian image classification using markov random fields. *Image and Vision Computing*, 14(4):285-295, 1996.

[11] L. Bruzzone and D. F. Prieto. Automatic analysis of the difference image for unsupervised change detection. *IEEE Transactions on Geoscience and Remote Sensing*, 38:3, 2000.

[12] Genderen C. Pohl J. L. Van. Review article multisensor image fusion in remote sensing: concepts, methods and applications. *International Journal of Remote Sensing*, 19(5):823-854, 1998. doi:10.1080/014311698215748.

[13] Warrender Christina E and Augusteijn Marijke F. Fusion of image classifications using bayesian techniques with markov random fields. *International Journal of Remote Sensing*, 20(10):1987-2002, 1999. doi:10.1080/014311699212308.

[14] John C.Price. Combining multispectral data of differing spatial resolution. *IEEE transactions on geoscience and remote sensing*, 37(3):1199–1203, 199.

[15] Schetselaar E. M. Fusion by the ihs transform: should we use cylindrical or spherical coordinates? *International Journal of Remote Sensing*, 19(4):759-765, 1998. doi:10.1080/014311698215982.

[16] Envi Users Guide. *The enviroment for visualizing images*, 4.1 edition, September 2004.

[17] Qiuming Cheng et.al. Principal component analysis with optimum order sample correlation coefficient for image enhancement. *International Journal of Remote Sensing*, 27, 2006.

[18] S. GEMAN and D. GEMAN. Stochastic relaxation, gibbs distributions, and the bayesian restoration of images. *IEEE Transactions on pattern analysis and machine intelligence*, 6:721741, 1984.

[19] Norway Gjøvik University College. Recent advances in acquisition and reproduction of multispectral images. 14th European Signal Processing Conference, EUSIPCO, 2006.

[20] Silander J. Zhou D. L. Civco J. A. A wavelet transform method to merge landsat tm and spot panchromatic data. *International Journal of Remote Sensing*, 19(4):743-757, 1998. doi:10.1080/014311698215973.

[21] T. Kasetkasem and P. K. Varshney. An image change detection algorithm based on markov random field models. *IEEE Transactions on Geoscience and Remote Sensing*, 40(8):18151823, 2002.

[22] C. De Boissezon H. LaporterieDejean, F. Latry. Evaluation of the quality of panchromatic/multispectral fusion algorithms performed on images simulating the future pleiades satellites. In GRSS/ISPRS, editor, *Remote Sensing and Data Fusion over Urban Areas*, pages 95- 98, Toulouse, France, 2003.

[23] Leica Geosystems, Atlanta, Georgia. *ERDAS IMAGINETour Guides*, 2003.

[24] Stan Z. Li. *Markov random field modeling in image analysis*. Computer science workbench. Springer, Tokyo, 2001.

[25] Q. LU and T. JIANG. Pixon-based image denoising with markov random fields. *Pattern Recognition*, 34:20292039, 2001.

[26] Brandt Tso; Paul M. Mather. *Classification methods for remotely sensed data*. Taylor and Francis, London, 2001.

[27] Paul M. Mather. *Computer Processing of remotely-sensed images, an introduction*. WILEY, 3 edition, 2004.

[28] Russell C.Hardie Michael T.Eismann. Application of the stochastic mixing model to hyperspectral resolution enhancement. *IEEE transactions on geoscience and remote sensing*, 42(9):1924–1933, 2004.

[29] R. T. Ogden. *Essential wavelets for statistical applications and data analysis*. Birkhauser, Boston etc., 1997.

[30] US Patent. Enhancing the resolution of multi-spectral image data with panchromatic image data using super resolution pan-sharpening. September 7,1999 http://www.patentstorm.us/patents/5949914claims.html.

[31] Christine Pohl. *Geometric aspects of multisensor image fusion for Topographic map updating in the humid tropics*. PhD thesis, International Institute for Aerospace Survey and Earth Sciences, 1996.

[32] A.K. Katsaggelos R. Molina, J. Mateos and R. ZuritaMilla. A new super resolution bayesian method for pansharpening landsat etm+ imagery. In *9th International Symposium on Physical Measurements and Signatures in Remote Sensing (ISPMSRS),*, 2005.

[33] K. Hailu Rahel. *Suitability of Markov random field based method for super resolution land cover mapping*. PhD thesis, ITC, 2006.

[34] R.E. Woods R.C. Gonzalez. *Digital image processing*. Prentice Hall, New-Jersey, 2 edition, 2002.

[35] A. H. S. Solberg, T. Taxt, and A. K. Jain. A markov random field model for classification of multisource satellite imagery. *IEEE Transactions on Geoscience and Remote Sensing*, 34(1):100-113, 1996.

[36] B. TSO and R. C. A OLSEN. A contextual classification scheme based on mrf model with improved parameter estimation and multiscale fuzzy line process. *Remote Sensing of Environment*, 97:127136, 2005.

[37] Veeraraghavan Vijayaraj. *A Quantitative Analysis of Pansharpened Images*. PhD thesis, Mississippi State University, 2004.

[38] R. W. Kiefer . W. J. Carper, T. M. Lillesand. The use of intensityhue-saturation transformations for merging spot panchromatic and multispectral image data. *Photogrammetric Engineering and Remote Sensing*, 56(4):459-467, 1990.

[39] L. Wald. Some terms of reference in data fusion. *IEEE Transactions on Geoscience and Remote Sensing*, 37(3):1190-1193, 1999.

[40] S.Richardson W.R.Gilks and D.J.Spiegelhalter. *Markov Chain Monte Carlo in practice*. CHAPMAN and HALL/CRC, second edition, 1998.

[41] Zhang Y. A new merging method and its spectral and spatial effects. *International Journal of Remote Sensing*, 20(10):2003-2014, 1999. doi:10.1080/014311699212317.

[42] Ruisheng Wang Yun Zhang. Multiresolution and multispectral image fusion for urban object extraction. *ISPRS, Journal of Geodesy and Geomatics Engineering*, 2004.

[43] Chen Yunhao, Deng Lei, Li Jing, Li Xiaobing, and Shi Peijun. A new waveletbased image fusion method for remotely sensed data. *International Journal of Remote Sensing*, 27(7):1465-1476, 2006. doi:10.1080/01431160500474365.

[44] Yun Zhang. Problems in the fusion of commercial high resolution satellite as well as landsat 7 images and initial solutions. *International Journal of Remote Sensing*, 2002.

[45] Yun Zhang and Gang Hong. An ihs and wavelet integrated approach to improve pansharpening visual quality of natural colour ikonos and quickbird images. *Information Fusion*, 6(3):225-234, 2005.

Appendix A

Summary of the result in searching optimal initial temperature (T_0) value

Table A.1: *Correlation summary of the result in searching optimal initial temperature (T_0) value*

W size	λ	σ	T_0	*Min Corr*	*Max Corr*	*Mean Corr*	*Std.Dev Corr*
1	0.1	0.5	0	0.9580282	0.9586282	0.9583282	0.00022624
			1	0.9609364	0.9620753	0.96159992	0.0004973
			2	0.9618629	0.9631862	0.96242552	0.0002262
			3	0.9619836	0.9627031	0.96229685	0.0002593
			4	0.9619633	0.9625361	0.96225689	0.0002208
			5	0.9607658	0.9630035	0.96217304	0.0006455
			7	0.9612298	0.9627546	0.96230447	0.0004518
			10	0.960962	0.962922	0.96223823	0.0006522
1	0.1	0.92	0	0.957706	0.957706	0.957706	0.0002212
			1	0.9629019	0.9652557	0.9649322	0.0011612
			2	0.9658113	0.9657213	0.9657113	0.0002208
			3	0.9648365	0.9652597	0.9652589	0.000436
			4	0.9656547	0.9642557	0.965249	0.0005306
			5	0.9650462	0.9651762	0.9650962	0.0006455
			7	0.9651729	0.9659729	0.9653729	0.0004518
			10	0.9652076	0.9658076	0.9655076	0.0006522

Table A.2: *RMSE summary of the result in searching optimal initial temperature (T_0) value*

W size	λ	σ	T_0	*Min RMSE*	*Max RMSE*	*Mean RMSE*	*Std.Dev RMSE*
1	0.1	0.5	0	1.1466592	1.1716592	1.166659	0.0056046
			1	1.1242532	1.1395927	1.13097	0.0065576
			2	1.1106902	1.128138	1.120252	0.0059007
			3	1.1171077	1.1263532	1.122230	0.00331
			4	1.118296	1.1260585	1.122469	0.0028908
			5	1.112816	1.1414252	1.123657	0.0082762
			7	1.1155855	1.1363835	1.121864	0.0060854
			10	1.1132722	1.138444	1.122402	0.0084304
1	0.1	0.92	0	1.0637922	1.17523275	1.17523275	2.575E-07
			1	1.07474	1.108631	1.07792125	0.0065576
			2	1.07030	1.07113325	1.07075825	0.0059007
			3	1.0761	1.07721	1.07716	0.0033104
			4	1.08770	1.0909585	1.0902085	0.0028908
			5	1.0791869	1.07956975	1.07936975	0.0082762
			7	1.0755001	1.075704	1.07552675	0.0060854
			10	1.0736370	1.073682	1.07365475	0.0084304

Table A.3: *Total Energy summary of the result in searching optimal initial temperature (T_0) value*

W size	λ	σ	T_0	*Min Energy*	*Max Energy*	*Mean Energy*	*Std.Dev Energy*
1	0.1	0.5	0	7.9543270	8.254327	8.154327	0.0230636
			1	7.939202	8.0176131	7.9863377	0.0308609
			2	7.908912	7.9732272	7.9338501	0.0220636
			3	7.901054	7.9903993	7.9553336	0.03218
			4	7.920197	7.9896782	7.9466349	0.0218070
			5	7.883887	8.0207221	7.9402165	0.0434745
			7	7.892586	8.0004859	7.9612818	0.0315737
			10	7.883724	8.0678443	7.9456258	0.0541798
1	0.1	0.92	0	7.455169	7.455169	7.455169	0.00000001
1	0.1		1	7.082704	7.175577	7.098468	0.046932835
1	0.1		2	7.067903	7.079671	7.07144	0.005450921
1	0.1		3	7.093962	7.045719	7.086371	0.00028345
1	0.1		4	7.099028	7.099368	7.099178	0.00023541
1	0.1		5	7.086128	7.086648	7.086448	0.000036345
1	0.1		7	7.074577	7.074887	7.074777	0.00036581
1	0.1		10	7.0394089	7.041589	7.070089	0.00006454

Appendix B

Summary of the result in searching optimal temperature updating factor (σ) value

Table B.1: *Correlation summary of the result in searching optimal temperature updating factor (σ) value*

W size	λ	σ	T_0	*Min Corr*	*Max Corr*	*Mean Corr*	*Std.Dev Corr*
1	0.1	0.1	2	0.9586095	0.9589333	0.95877398	0.0001241
		0.2		0.958967	0.959982	0.9594563	0.0004760
		0.3		0.959703	0.960591	0.96015517	0.0002788
		0.4		0.960887	0.9616656	0.96134137	0.0003143
		0.5		0.9612298	0.9627546	0.96230447	0.0004518
		0.6		0.9624038	0.9633909	0.96303116	0.0003213
		0.7		0.963412	0.9643005	0.96398606	0.000295
		0.8		0.9641057	0.9648907	0.96452816	0.0002394
		0.9		0.9636454	0.9650149	0.9645404	0.0004041
		0.91		0.9625596	0.9659714	0.964581	0.0011116
		0.92		0.9645943	0.9656445	0.96490592	0.0003618
		0.93		0.9636195	0.9649758	0.96470552	0.0004043
		0.94		0.9646164	0.9651166	0.9648260	0.0002401
		0.95		0.9640868	0.965166	0.9648926	0.0003498
		0.96		0.9645127	0.964853	0.9646803	0.0001498
		0.97		0.9643592	0.9648766	0.9647163	0.0001842
		0.98		0.961172	0.9636255	0.9633068	0.0007536
		0.99		0.94669	0.954876	0.95314025	0.0024428

Table B.2: *RMSE summary of the result in searching optimal temperature updating factor (σ) value*

W size	λ	σ	T_0	*Min RMSE*	*Max RMSE*	*Mean RMSE*	*Std.Dev RMSE*
1	0.1	0.1	2	1.163709	1.169034	1.1662323	0.0020350
		0.2		1.151137	1.16365875	1.1578356	0.0057522
		0.3		1.143715	1.15450875	1.1492767	0.00343903
		0.4		1.130161	1.14008975	1.1345413	0.0041116
		0.5		1.11558	1.1363835	1.1222301	0.0060735
		0.6		1.106567	1.1205815	1.1121229	0.0045350
		0.7		1.09560	1.1068855	1.0992459	0.0039064
		0.8		1.086889	1.09774275	1.09181	0.0032449
		0.9		1.085000	1.10322675	1.0914245	0.0054693
		0.91		1.06027	1.0911935	1.0849692	0.009428
		0.92		1.05526	1.16433	1.0965703	0.0371254
		0.93		1.08575	1.08909725	1.0876892	0.001677
		0.94		1.068183	1.090101	1.0842318	0.0080659
		0.95		1.081755	1.08924075	1.0854353	0.0033016
		0.96		1.075635	1.091104	1.0880293	0.0047502
		0.97		1.077721	1.090316	1.0872982	0.0037915
		0.98		1.102536	1.12099975	1.10536485	0.0055795
		0.99		1.21117	1.30408025	1.2322389	0.0278210

Table B.3: *Total Energy summary of the result in searching optimal temperature updating factor (σ) value*

W size	λ	σ	T_0	*Min Energy*	*Max Energy*	*Mean Energy*	*Std.Dev Energy*
1	0.1	0.1	2	8.145959	8.212977	8.1698326	0.029334322
		0.2		8.100198	8.201726	8.1495455	0.036536237
		0.3		8.012684	8.123748	8.0888326	0.033085087
		0.4		8.012603	8.06742	8.0339669	0.022801959
		0.5		7.892586	8.000489	7.9612818	0.031573751
		0.6		7.863724	7.973175	7.9058323	0.030914496
		0.7		7.810591	7.874166	7.8489842	0.019762046
		0.8		7.770852	7.851354	7.8243611	0.024281307
		0.9		7.774204	7.886612	7.8057648	0.032386118
		0.91		7.802071	7.80944	7.8079662	0.003107043
		0.92		7.765513	7.802782	7.7766937	0.018002637
		0.93		7.799816	7.80944	7.8019059	0.002874595
		0.94		7.786323	7.81049	7.7994622	0.007487957
		0.95		7.779575	7.794638	7.7856002	0.0077785
		0.96		7.777784	7.786278	7.7811816	0.004386283
		0.97		7.776494	7.791842	7.784168	0.008089106
		0.98		7.998144	8.029534	8.016978	0.016209726
		0.99		6.152043	9.217615	8.9110578	0.969418985

Appendix C

Summary of the result in searching optimal smoothness parameter (λ) value

Table C.1: *Correlation summary of the result in searching optimal smoothness parameter (λ) value*

W size	λ	σ	T_0	*Min Corr*	*Max Corr*	*Mean Corr*	*Std.Dev Corr*
1	0	0.92	2	0.4398918	0.4398918	0.4398918	0.0000001
	0.02			0.926916	0.9356916	0.9296916	0.0000132
	0.04			0.9656916	0.9656916	0.9656916	0.0000002
	0.05			0.9644566	0.9651371	0.965001	0.0002869
	0.06			0.9641655	0.9657046	0.96447077	0.0006435
	0.07			0.963627	0.9641000	0.9640527	0.0001495
	0.08			0.9652785	0.9654151	0.96540144	0.0000431
	0.09			0.9653478	0.9657411	0.96570177	0.0001243
	0.1			0.9636454	0.9650149	0.96453534	0.0003994
	0.2			0.959411	0.959928	0.95964016	0.0001630
	0.3			0.952574	0.9529865	0.95271985	0.0001339
	0.4			0.9428412	0.9435805	0.94322817	0.0002569
	0.5			0.931571	0.932347	0.93193063	0.0002638
	0.6			0.9154313	0.9169585	0.91648949	0.0004605
	0.7			0.8955123	0.8968364	0.89631978	0.0003836
	0.8			0.8662926	0.8692356	0.86751133	0.0008358
	0.9			0.4407393	0.4722589	0.45294568	0.0111206

Table C.2: *RMSE summary of the result in searching optimal smoothness parameter (λ) value*

W size	λ	σ	T_0	*Min RMSE*	*Max RMSE*	*Mean RMSE*	*Std.Dev RMSE*
1	0	0.92	2	7.36081	7.82126	7.775221	0.145609
	0.02			1.65863025	1.69561	1.670608	0.1161435
	0.04			1.06418975	1.06418	1.064189	0.000000
	0.05			1.064355	1.07341	1.066167	0.0038214
	0.06			1.05970225	1.0808165	1.0739829	0.0092222
	0.07			1.0844425	1.0911935	1.0857927	0.0028464
	0.08			1.07059425	1.072672	1.0710098	0.0008760
	0.09			1.05033875	1.070338	1.0605216	0.0103535
	0.1			1.08500075	1.103226	1.0915538	0.0053552
	0.2			1.2083855	1.213932	1.2113233	0.0022137
	0.3			1.35271725	1.355803	1.3545954	0.0010446
	0.4			1.50790875	1.515209	1.5119084	0.002102
	0.5			1.67048125	1.676060	1.673345	0.002091
	0.6			1.8390735	1.853143	1.8469516	0.004691
	0.7			2.037615	2.045479	2.0413018	0.002271
	0.8			2.26483825	2.27183	2.2674132	0.002359
	0.9			3.9325775	3.992317	3.96320	0.020339

Table C.3: *Total Energy summary of the result in searching optimal smoothness parameter (λ) value*

W size	λ	σ	T_0	*Min Energy*	*Max Energy*	*Mean Energy*	*Std.Dev Energy*
1	0	0.92	2	0.1319531	0.1335547	0.13323438	0.0006752
	0.02			7.98453	7.98453	7.98453	0.0000001
	0.04			7.774204	7.886612	7.8126632	0.0365193
	0.05			7.769162	7.886612	7.8056632	0.0351686
	0.06			7.703315	7.886612	7.7986632	0.0470273
	0.07			7.593315	7.886612	7.7876632	0.0758439
	0.08			7.586612	7.831791	7.7776632	0.0696516
	0.09			7.064641	7.091802	7.0727893	0.0131200
	0.1			7.774204	7.886612	7.8076632	0.0333857
	0.2			14.07973	14.17549	14.140082	0.0323363
	0.3			18.69675	18.76753	18.729927	0.0290312
	0.4			21.44002	21.62196	21.486313	0.0631378
	0.5			22.42546	22.58708	22.502362	0.0565199
	0.6			21.85669	22.01999	21.965036	0.0553243
	0.7			19.82025	19.96852	19.902638	0.0448577
	0.8			16.3031	16.38765	16.345806	0.0276877
	0.9			0.2039039	0.276329	0.24676946	0.0262192

Appendix D

Summary of the result in searching optimal window size value

Table D.1: *Correlation summary of the result in searching optimal Window size (W_size) value*

W size	λ	σ	T_0	*Min Corr*	*Max Corr*	*Mean Corr*	*Std.Dev Corr*
1	0.09	0.92	2	0.9653478	0.96574	0.965701	0.000124
3				0.9632565	0.9635844	0.963333	0.000133
5				0.9624084	0.962637	0.9624982	0.000083
7				0.9617742	0.962146	0.961927	0.000165
W size	λ	σ	T_0	*Min RMSE*	*Max RMSE*	*Mean RMSE*	*Std.Dev RMSE*
1	0.09	0.92	2	1.050338	1.070338	1.0605216	0.010353
3				1.13395	1.13901	1.1376743	0.001375
5				1.16286	1.165201	1.16460	0.000941
7				1.18207	1.185755	1.184171	0.001776
W size	λ	σ	T_0	*Min Energy*	*Max Energy*	*Mean Energy*	*Std.Dev Energy*
1	0.09	0.92	2	7.064641	7.091802	7.0727893	0.013120
3				12.10074	12.1376	12.117737	0.015746
5				14.35663	14.41622	14.39888	0.024488
7				15.81269	15.85634	15.823796	0.017421

Appendix E

Summary of the result in searching optimal initial temperature (T_0) value using optimal values from synthetic data II

Table E.1: *Correlation summary of the result in searching optimal initial temperature (T_0) value using optimal values obtained from synthetic image II*

W size	λ	σ	T_0	*Min Corr*	*Max Corr*	*Mean Corr*	*Std.Dev Corr*
1	0.09	0.92	0	0.957706	0.957706	0.957706	0.000221245
			1	0.9629019	0.9652557	0.9649322	0.001161226
			2	0.9658113	0.9657213	0.9657113	0.000220835
			3	0.9648365	0.9652597	0.9652589	0.00043634
			4	0.9656547	0.9642557	0.965249	0.000530663
			5	0.9650462	0.9651762	0.9650962	0.000645502
			7	0.9651729	0.9659729	0.9653729	0.000451869
			10	0.9652076	0.9658076	0.9655076	0.000652288

Table E.2: *RMSE summary of the result in searching optimal initial temperature (T_0) value using optimal values obtained from synthetic image II*

W size	λ	σ	T_0	*Min RMSE*	*Max RMSE*	*Mean RMSE*	*Std.Dev RMSE*
1	0.09	0.92	0	1.06379225	1.17523275	1.17523275	2.575E-07
			1	1.0747455	1.108631	1.07792125	0.006557664
			2	1.0703075	1.07113325	1.07075825	0.005900717
			3	1.076135	1.07721	1.07716	0.003310401
			4	1.0877085	1.0909585	1.0902085	0.002890837
			5	1.079186975	1.07956975	1.07936975	0.008276271
			7	1.075500175	1.075704	1.07552675	0.006085496
			10	1.073637025	1.073682	1.07365475	0.008430447

Table E.3: *Total Energy summary of the result in searching optimal initial temperature (T_0) value using optimal values obtained from synthetic image II*

W size	λ	σ	T_0	*Min Energy*	*Max Energy*	*Mean Energy*	*Std.Dev Energy*
1	0.09	0.92	0	7.455169	7.455169	7.455169	0.00000003
			1	7.082704	7.175577	7.098468	0.046932835
			2	7.067903	7.079671	7.07144	0.005450921
			3	7.093962	7.045719	7.086371	0.00028345
			4	7.099028	7.099368	7.099178	0.00023541
			5	7.086128	7.086648	7.086448	0.000036345
			7	7.074577	7.074887	7.074777	0.00036581
			10	7.0394089	7.041589	7.070089	0.00006454